Phenotypic characterization of *HAM1*, a novel mating regulator of the fungal pathogen *Cryptococcus neoformans*.

Elizabeth Arsenault Yee[1], Robbi L. Ross[1], Felipe H. Santiago-Tirado[1,2,3,*]

[1]Department of Biological Sciences, University of Notre Dame, Notre Dame, Indiana 46556

[2]Eck Institute for Global Health, University of Notre Dame, Notre Dame, Indiana 46556

[3]Warren Center for Drug Discovery, University of Notre Dame, Notre Dame, Indiana 46556

*Address correspondence to this author at fsantiago@nd.edu

Running title: A novel negative regulator of mating in *C. neoformans*

Keywords: *Cryptococcus neoformans*, Fungal mating, Polysaccharide capsule

Word count (excluding Methods, References, tables, and legends): 4,985

Abstract: 250 words

Cryptococcus neoformans is a fungal pathogen responsible for >200,000 yearly cases with a mortality as high as 81%. This burden results, in part, from an incomplete understanding of its pathogenesis and ineffective antifungal treatments, hence there is a pressing need to understand the biology and host interactions of this yeast to develop improved treatments. Characterization of genes of unknown function can provide a better understanding of cryptococcal biology and open possible avenues for more effective treatments. Protein palmitoylation is important for cryptococcal virulence, and we previously identified the substrates of its main palmitoyl transferase. One of these substrates was encoded by the uncharacterized gene CNAG_02129. This gene has a partially characterized homolog in the filamentous fungus *Neurospora crassa* named *HAM13,* where it plays a role in proper cellular communication and filament fusion. In *Cryptococcus*, cellular communication is essential during mating, therefore we hypothesized that CNAG_02129, which we named *HAM1,* may play a role in mating. We found that *ham1Δ* mutants produce more progeny during mating, filament more robustly, and exhibit competitive fitness defects under mating and non-mating conditions. Consistent with previous reports that have linked changes in mating to altered virulence capacity, we found several differences with the major virulence factor, the polysaccharide capsule. We observed that *ham1Δ* mutants have decreased capsule attachment and transfer but exhibit higher amounts of exopolysaccharide shedding and biofilm production. Understanding the connection between mating and virulence in *C. neoformans* may open new avenues of investigation into ways to improve the treatment of this disease.

39 **Importance:** 146 words

40 Fungal mating is a vital part of the lifecycle of the pathogenic yeast *Cryptococcus*
41 *neoformans*. More than just ensuring the propagation of the species, mating allows for
42 genetic diversity as well as the generation of infectious particles that can invade mammalian
43 hosts. Despite its importance in the biology of this pathogen, we still do not know all of the
44 major players regulating the mating process and if they are involved or impact its
45 pathogenesis. Here we identified a novel negative regulator of mating that also affect certain
46 characteristics know to be important for virulence. This gene, which we call *HAM1*, is widely
47 conserved across the cryptococcal family as well as in many pathogenic fungal species. This
48 study will open new avenues of exploration regarding the function of uncharacterized but
49 conserved genes in a variety of pathogenic fungal species, and specifically in serotype A of
50 *C. neoformans*.

1. Introduction:

There are approximately 6 million fungal species worldwide (Fisher et al., 2020), and although most play beneficial roles in their environments, a few hundred are known to be pathogenic to mammalian hosts (Fisher et al. 2020). A common theme in these fungal infections is the importance of morphological transitions for pathogenesis. *Histoplasma capsulatum* grows naturally as a mold in the environment but under host conditions, it grows as a budding yeast which allows for greater dissemination in the bloodstream (Min et al., 2020). Conversely, *Aspergillus fumigatus* conidia are inhaled into the lungs and germinate into hyphal filaments, which can form mycelial networks that are able to invade into host tissues and due to their large size, are unable to be phagocytosed by host immune cells (Min et al., 2020). In the case of *Cryptococcus neoformans*, one such morphological transition happens prior to host invasion, where sexual and asexual reproduction produces spores which are infectious agents inhaled into the lungs to establish infection.

C. neoformans is an opportunistic basidiomycete pathogenic fungus present worldwide (Srikanta D et al, 2014). Because it is in the environment, desiccated yeasts and spores are frequently inhaled into the lungs, causing an infection that in healthy individuals is controlled and remains asymptomatic until cleared. However, in the immunocompromised, the infection quickly overwhelms the immune system in the lungs, resulting in pneumonia and acute respiratory distress syndrome, with subsequent dissemination to the central nervous system causing lethal meningoencephalitis (Maziarz and Perfect, 2016). *C. neoformans* is a leading cause of death in HIV/AIDS, where there are approximately 152,000 cases each year with 112,000 resulting in death (Rajasingham et al., 2022). This staggering mortality rate stems largely from a lack of effective treatment options as well as an incomplete understanding of cryptococcal pathogenesis. This has prompted the World Health Organization to include *C. neoformans* in their highest critical priority group in its recent Fungal Priority Pathogen List (World Health Organization, 2022).

In a previous study investigating fungal factors necessary for phagocyte recognition and internalization (Santiago-Tirado et al., 2015), we identified a gene homologous to *Saccharomyces cerevisiae*'s Protein Fatty Acyltransferase 4 (*PFA4*). We and others showed that cryptococcal *PFA4* was necessary for complete virulence in a mammalian host (Santiago-Tirado et al., 2015, Nichols et al., 2015). Since palmitoyl acyl transferases (PAT)

82 like Pfa4 act by modifying substrate proteins, we determined its palmitoylome. Using
83 comparative mass spectrometry between wild-type (WT) and *pfa4*Δ samples to determine
84 downstream targets, one of the most highly enriched substrates was encoded by the gene
85 of unknown function CNAG_02129 (Santiago-Tirado et al., 2015).

86 CNAG_02129 is part of a conserved family of fungal genes of which only one member, from
87 the filamentous ascomycete *Neurospora crassa*, has been partially characterized (hyphal
88 anastomosis protein 13 (HAM-13); Dettmann A et al., 2014)(Fig. 1A). In the absence of HAM-
89 13, only 33% of the *N. crassa* germlings find each other and fuse. This is in stark contrast to
90 almost 100% of the WT germlings finding each other, undergoing cellular fusion, and mature
91 into interconnected hyphae to form a mycelium (Fischer et al., 2019). Thus, the authors
92 concluded that HAM-13 plays a role on cellular communication. In *C. neoformans*, this type
93 of cellular communication is essential for mating, which can be either unisexual or bisexual
94 depending on the surrounding environmental pressures such as nutrient limitation or
95 pheromone secretion. Members of the *C. neoformans* species complex have two mating
96 types determined by the MAT locus, MATα and MATa. In a bisexual scenario, MATα and
97 MATa cells find each other through pheromone signaling, which triggers a cell fusion event
98 resulting in a morphological transition into filamentous hyphae. The nucleus from each parent
99 travels up these hyphal structures to the apex where a basidia is formed. Within the basidia,
100 nuclear fusion occurs followed by meiosis and several rounds of mitosis to produce four
101 chains of haploid basidiospores. These spores then drop from the basidium and mature into
102 yeast where the process can be started again. In a unisexual scenario, the same events
103 occur but only in cells containing the MATα loci (Wickes, 2002, Zhao and Lin 2021). Almost
104 all of these details, however, are from studies using serotype D *C. neoformans* (now called
105 *C. deneoformans*), and considerably less is known about *C. neoformans* strains that are
106 serotype A (*C. neoformans sensu stricto*).

107 Several studies have shown an inverse relationship between *C. neoformans's* virulence and
108 its filamentous mating form (Lin 2009). For example, when *ZNF2,* a master regulator of
109 filamentation in *C. neoformans*, is constitutively overexpressed, the cells are morphologically
110 hyphal-locked and unable to cause disease in a mouse model (Wang et al., 2012). These
111 hyphal-locked cells induced a protective TH-1 pro-inflammatory immune response that not
112 only resulted in full clearance of the initial infection, but also protection from subsequent
113 challenges (Zhai et al., 2015). This suggests that mating regulators may also play a larger

114 role in control of virulence mechanisms, such as impacting anyone of the main cryptococcal
115 virulence factors, its polysaccharide capsule, growth at human body temperature, and
116 melanization. These and other factors allow for *C. neoformans* to persist within the harsh
117 environment of a human host. While each of these virulence mechanisms has been
118 comprehensively studied, not all the regulators have been uncovered.

119 In this study, we determined that CNAG_02129, which we refer as *HAM1* (Hyphal
120 anastomosis protein 1), plays a role in cryptococcal mating by acting as a negative regulator
121 of mating, and has a connection to proper release of the polysaccharide capsule that may
122 affect virulence. With our *ham1*Δ strains we observed increased cellular fusion with and
123 without exogenous pheromone, a hyper hyphal response during bisexual mating scenarios,
124 and reduced competitive fitness under both mating and non-mating conditions. Interestingly,
125 these effects were specific for *C. neoformans* (serotype A) and were not obvious in *C.*
126 *deneoformans* (serotype D), highlighting the known differences in mating regulation between
127 the sister species. Consistently, we found trends of differences in MATα pheromone loci
128 expression over time in unilateral and bilateral crosses. Although we do not observe major
129 defects in capsule generation and other key virulence mechanisms, we found defects in
130 capsule attachment, an increase in capsule shedding, less effective capsule transfer, and an
131 increase in biofilm production. These findings suggest a connection between mating and
132 proper capsule formation and shedding, which can impact the virulence potential of this
133 organism, as well as contribute to our understanding of mating regulation in this important
134 fungal pathogen.

135 **2. Results**

136 **2.1 Ham1 is a palmitoylated protein conserved across the fungal kingdom**

137 To confirm the results of our previous large scale Pfa4 palmitoylome studies we investigated
138 the palmitoylation status of Ham1. Using a *HAM1*-FLAG tagged strain (see Methods) we
139 performed an immunoprecipitation coupled with click-chemistry to determine if the Ham1
140 protein was palmitoylated. We confirmed that Ham1 is palmitoylated by the presence of a
141 fluorescent band only in the palmitate fed fraction of our Ham1-FLAG IP that was at the same
142 size as the accompanying western blot (Fig 1B, C). Next, we wanted to see if the
143 palmitoylation modification may be conserved across the protein homologs. Using the

144 palmitoylation predictor software GPS-Palm (Ning et al., 2020), we determined that all of the
145 homologs investigated had very high confidence predictions for palmitoylation (Fig 1D).

146 **2.2 *ham1Δ* exhibits altered cellular fusion and progeny with a dry colony morphology.**

147 The goal of mating is to produce viable progeny with traits from both parents, generating
148 better-adapted cells (Fu et al., 2019). This requires that parental strains find each other, fuse,
149 undergo recombination, and then produce haploid spores. To test if mating was affected,
150 deletion strains of *HAM1* were generated in both mating types of the KN99 background (WT)
151 using different resistance markers (G418 or NAT). We then set up mating crosses between
152 KN99α x KN99a, KN99a x *ham1*Δα, and KN99α x *ham1*Δa, and determine the fusion
153 efficiency from the number of colonies resistant to both antibiotics. Both *ham1*Δ mutant
154 crosses yielded significantly higher progeny resistant to both antibiotics when compared to
155 the WT cross, indicating faster, or more efficient, cellular fusion (Fig. 2A, Supplemental 1B).
156 To explore the impact that pheromone has on cellular fusion we tested if adding synthetic
157 exogenous pheromone would increase the rate of cell fusion in our *ham1*Δ mutants (Fig. 2A).
158 Although addition of exogenous pheromone to the WT cross resulted in an increase in the
159 number of progeny generated, there was no significant difference in the fusion rate
160 (Supplemental 2A). In contrast, in our *ham1*Δ crosses we saw slight increases in double-
161 positive progeny that was dose-dependent, reaching statistical significance at 7.5μM
162 exogenous pheromone and trending towards significance at 5 and 10μM (Supplemental 2B,
163 C). This suggests that the *ham1*Δ crosses are more sensitive to exogenous pheromone.
164 Interestingly, when scoring double-resistant progeny, we observed a difference in the colony
165 morphology. Rather than the typical glossy, round shape colonies of WT strains, the progeny
166 from the *ham1*Δ crosses had a dry, irregular morphology (Fig. 2B). When resuspending
167 single colonies from these crosses and staining them with DAPI and CFW to visualize, we
168 found that these colonies were comprised of the hyphal form of *Cryptococcus,* as the septal
169 divisions and a bi-nuclear distribution along septa were evident (Fig. 2B). In contrast, the
170 colonies from the WT crosses only showed budding yeasts. This drastic increase in the ability
171 to fuse as well as the dry appearance and hyphal state of *ham1*Δ progeny led us to consider
172 what other facets of the mating cycle could be altered.

173 **2.3 *ham1*Δ mutants have increased hyphal production in bisexual mating scenarios**
174 **on V8 medium.**

175 Hyphal growth is a quantitative trait that can be used to measure how well a strain is able to
176 mate (Fu et al., 2019). We assessed the ability of our *ham1*Δ crosses to form hyphae in a
177 time course from 5 days to 4 weeks. We observed faster and more robust filamentation in
178 our *ham1Δ* crosses across all time points (Fig. 3A, Supplemental 1A). When quantifying the
179 hyphal area, we observed a significant increase in all unilateral mutant crosses at 5 days and
180 3 weeks, and a significant increase in the hyphal area of the bilateral crosses across all time
181 points (Fig 3B). This was confirmed using two other independent *ham1Δ* mutants, including
182 one from the deletion collection available commercially (www.fgsc.net; Supplemental 1).

183 **2.4 *ham1*Δα strain exhibits a fitness disadvantage in both mating and non-mating**
184 **scenarios.**

185 Mating is an energy costly process, and may result in a fitness cost when comparing mating
186 and non-mating conditions. However, this is crucial for survival in the environment where
187 mating partners are few and far between and the pressures of predators and other stressors
188 threaten survival. We tested if our *ham1*Δ would display increased fitness compared to a WT
189 competitor due to its propensity to form more hyphae and increased cellular fusion events.
190 To test this, we had two MATα or two MATa strains with opposing resistance cassettes (the
191 competitors) co-incubated with the opposing mating type with no resistance cassette (the
192 donor) (Fig. 4A). All three strains were plated under mating (V8) or non-mating (YPD)
193 conditions for 10 days. At that point, each competitive scenario was scraped, resuspended,
194 and plated on selective media to determine the colony forming units (CFUs) of each
195 competitor (Fig. 4A). In the mating permissive condition (V8) we expect both competitors to
196 stop vegetative budding and forage for mating partners while in the non-mating condition
197 (YPD) we expect both competitors to simply divide. In the WT cross we observed no
198 difference in competitive fitness in either YPD or V8 media conditions (Fig. 4B). However, in
199 our *ham1*Δα competition we saw a dramatic reduction in the competitive fitness of the
200 *ham1*Δα in both the V8 and YPD conditions (Fig. 4C). Surprisingly, in our *ham1*Δa
201 competition we observed a slight competitive advantage in YPD and no competitive
202 difference in V8 (Fig. 4D).

203 **2.5 Transcriptional analysis of MATα, MATa and *HAM1* over time.**

204 To determine if *HAM1* is involved in the pheromone response MAP kinase pathway we
205 analyzed the transcriptional activity of the MATα/MATa pheromone loci and *HAM1* under

206 YPD and V8. This type of analysis is typically done in *C. deneoformans* (serotype D), but
207 when we deleted *HAM1* in this species, mating was unaffected. Since it is known that there
208 are differences in mating regulation between the two sister species, we decided to continue
209 and analyze the transcription of these genes in *C. neoformans* (serotype A). To do this for
210 the pheromone loci, we compared the gene expression of MATα and MATa in mating
211 conditions normalized to the expression in non-mating conditions to get the relative fold
212 induction (Son et al., 2019, Viviani et al., 2001). We performed this in a time course of 1, 3,
213 5 and 7 days to look at changes in expression over time (Fig. 5 A-C). While we observed no
214 statistically significant differences in pheromone expression in either MATα or MATa, we saw
215 that the *ham1*Δα unilateral cross trends towards higher MATα pheromone expression at days
216 1, 3 and 5 and returns to WT levels at day 7. For *HAM1* we looked at fold induction in non-
217 mating and mating conditions to see how transcription changed over time. We saw that at
218 day 1 in non-mating conditions *HAM1* had a much higher expression as compared to mating
219 conditions (Fig. 5C). However, as the mating cycle progressed, we observed higher
220 expression of *HAM1* in mating conditions relative to non-mating conditions at days 3 and 5
221 with a final leveling off in both conditions by day 7 (Fig. 5C). These findings suggest that
222 *HAM1* may be acting as an early mating cycle checkpoint.

223 **2.6 *ham1Δ* has no significant defects in major virulence mechanisms.**

224 So far, all the phenotypes of the *ham1*Δ have been mating related, especially in the MATα
225 background. We wondered if these would also affect virulence, hence we investigated if there
226 were defects in the main virulence factors of *C. neoformans*: capsule production, ability to
227 melanize, thermotolerance (37°C), and recognition by phagocytic cells (Fig. 6). We found no
228 major differences in any of the major virulence mechanisms (Fig. 6, Supplemental 1). Due to
229 the surface defects observed in the *pfa4*Δ mutant (Ham1's PAT) we wanted to take a closer
230 look at the cell wall and the capsule of our *ham1Δ* strains as more nuanced differences could
231 be present besides capsule induction. Finding no apparent defects under different cell wall
232 and membrane stressors (Supplemental 3), we took a closer look at the polysaccharide
233 capsule and investigated differences in its attachment and release.

234 **2.7 *ham1Δ*α exhibits defects in capsule attachment and transfer.**

235 First, we looked at capsule attachment. After inducing capsule formation, we subjected WT,
236 *ham1*Δα and a known capsule mutant (*pbx1*Δ) to sonication (Fig. 7A). We found that our

237 *ham1*Δα mutant lost significantly more capsule than WT cells, suggesting a defective
238 attachment to the cell wall (Fig. 7B, Supplemental 1). The next avenue we investigated was
239 capsule transfer. We incubated the acapsular mutant *cap59*Δ with conditioned media from
240 WT, *ham1*Δα, *pbx1*Δ and *cap59*Δ to see how well the capsular material could attach to the
241 cell wall of *cap59*Δ. As expected, our *cap59*Δ mutant could not transfer capsule at any dilution
242 tested due to the lack of capsule. Our *pbx1*Δ mutant also was unable to transfer capsule at
243 dilutions higher than 1:5 which was unsurprising due to its known capsule defects (Liu et al.,
244 2007, Kumar et al., 2014). However, our *ham1*Δα also struggled to transfer the capsule at
245 higher dilutions >1:750, whereas the WT capsule had no problem at these dilutions. This
246 indicates at least a small defect in either structure or reduced release of capsule (Fig. 7C,
247 Supplemental 1). Defects indicated by sonication and transfer in our *ham1*Δα prompted us
248 to look at shedding and biofilm production which could further confirm issues with capsular
249 release (Denham et al., 2018)

250 **2.8 *ham1Δ*α has altered capsule shedding in different medias and higher biofilm**
251 **production.**

252 To investigate the possibility of defects with capsule release, we assessed the ability of
253 *ham1*Δα to shed capsule in different medias by electrophoresis and immunoblotting (Yoneda
254 and Doering, 2008, Denham et al., 2018) (Fig. 8A). We observed specific differences in the
255 shed polymer size in nutrient-rich YPD medium with potential differences in size and amount
256 in the capsule inducing medium DMEM and the minimal growth medium YNB (Fig. 8A). To
257 get a more quantitative measurement of amounts sheds, we measured GXM concentration
258 by ELISA (Denham et al., 2018). In YPD we saw a significant increase in the amount of
259 capsule shed in our *ham1*Δα (Fig. 8B, Supplemental 1). We saw no significant difference in
260 the amount of capsule material shed in YNB or DMEM relative to WT, although in both there
261 was a trend towards higher capsule shedding in our *ham1*Δα (Fig 8. B-D, Supplemental 1).
262 For all medias, our capsule shedding mutant *pbx1Δ* shed less than WT, as expected, and
263 our a capsular mutant *cap59Δ* did not shed any capsule. Given the association between
264 capsule and biofilm formation, we next assessed how well *ham1*Δα could produce a biofilm
265 using the XTT biofilm assay (Pierce, et al., 2008). We found that our *ham1*Δα produced larger
266 biofilms than our WT as did *pbx1Δ* whereas no biofilm was produced in the acapsular mutant
267 *cap59Δ* (Fig. 8E).

268 **2.9 *ham1Δα* shows no difference in virulence capacity in *G. mellonella.***

269 Lastly, to investigate whether the role of *HAM1* in mating and proper capsule function
270 translates to virulence defects, we performed infections using the invertebrate model system
271 *Galleria mellonella*. We infected G. *mellonella* with $1x10^5$ log phase cells/larvae and,
272 surprisingly, saw no significant difference between WT and independent *ham1Δα* mutants
273 (Fig. 9A, Supplemental 1). On the other hand, the *pbx1*Δ mutant showed attenuated virulence
274 which is consistent with previous studies (Liu et al., 2007). We also assessed fungal burden
275 at time of death, but saw no significant difference in the fungal burden of any of the strains
276 (Fig. 9B, Supplemental 1).

277 **3. Discussion**

278 Mating is a vital part of the lifecycle of *C. neoformans.* It allows for increased genetic diversity
279 among progeny and overall propagation of the species. Despite having a well-defined sexual
280 cycle both in unisexual and bisexual scenarios, not all the important regulators of mating are
281 known, especially in serotype A strains. Our results presented here are consistent with *HAM1*
282 acting as a negative regulator of mating specifically in *C. neoformans*, with additional direct
283 or indirect roles pertaining to the capsule. Moreover, mating has been suggested to impact
284 infection in multiple ways, hence understanding how it is regulated may yield novel and more
285 effective ways to prevent, or treat, this disease.

286 Given the proposed role of HAM-13 in *N. crassa*, we focused on the ability of cryptococcal
287 *ham1*Δ mutants to fuse and produce recombinant progeny. Throughout our investigations,
288 *ham1Δ* mutants consistently outperformed the WT strain in hyphal formation and production
289 of progeny. This suggests that *HAM1*, like its homolog in *N. crassa*, is somehow connected
290 to the filamentation process in fungal mating and cell-to-cell communication. However, these
291 phenotypes were only present in *C. neoformans* and not in *C. deneoformans*, precluding us
292 from interrogating more in depth the potential signaling pathways affected by *HAM1*. Mating
293 studies in *Cryptococcus* have been mostly done in serotype D strains (*C. deneoformans*)
294 rather than in serotype A, as in this study, because of the natural propensity for mating in *C.*
295 *deneoformans*. Hence, although surprising, it is not unexpected that *HAM1* deletion yields
296 different phenotypes between the sister species. Additionally, we found the *HAM1* effects
297 were exclusively found in the V8 mating inducing medium as there was no significant
298 increase in the amount of filamentation observed in either Musharige-Skoog (MS) or

299 Filamentation Agar (Supplemental 4). V8 media is considered the “gold standard” for looking
300 at mating interactions in *C. neoformans*, while the others are mostly used in *C. deneoformans*
301 (Sun et al., 2019), potentially explaining why we only see phenotypes in V8. Given that mating
302 in *C. neoformans* is less well understood, and considering the larger epidemiological impact
303 of serotype A strains which comprise 95% of clinical isolates and have been associated with
304 higher virulence potential (Lin, 2008, Barchiesi et al., 2005), we chose to remain in the
305 serotype A strain for these mating assessments.

306 The potential role of *HAM1* in filamentation was very apparent in our *ham1Δ* cellular fusion
307 progeny, which exhibited a dry desiccated form which were in fact aggregates of hyphae.
308 However, when these dry colonies were re-streaked, they returned to a “normal” colony
309 morphology. The presence of the filamentous form in the absence of any mating pressure
310 shows that the progeny of our *ham1*Δ strains have an even stronger drive towards the mating
311 form but that over time, the signaling to return to a normal yeast state is reestablished. This,
312 however, could impact the fitness of these strains under non-mating conditions. Thus, we
313 were surprised to find that our *ham1Δ*α has a fitness disadvantage in both mating permissive
314 and non-mating conditions, whereas our *ham1*Δa performed similarly in mating permissive
315 and slightly better in non-mating conditions. One of the main differences between cellular
316 competition and other classical mating assays in *C. neoformans* is that in the latter, opposite
317 mating type partners are in very close proximity which masks issues with searching for mating
318 partners. In our *ham1*Δα competitions under mating conditions, *ham1*Δα while good at
319 making hyphae and producing progeny with a close proximity partner, may lack the ability to
320 effectively forage for mating partners in nonstatic conditions. The disadvantage in non-mating
321 conditions may be the result of two possibilities. First, *ham1*Δα has a drive to mate that
322 outweighs the drive to cellularly divide in the presence of an opposite mating partner. Second,
323 in *S. cerevisiae* prolonged exposure to mating pheromones results in programmed cell death
324 (Severin, et al., 2002). This same principle may apply to *C. neoformans* in that the presence
325 of an opposite mating partner and the generation of MATα pheromone may induce inhibition
326 of cellular growth or death in *ham1*Δα cells. Surprisingly, in our *ham1*Δa competition, we
327 observed a slight increase in competitive fitness in non-mating conditions and no difference
328 in mating conditions. These observations may be the result of the differences in the
329 morphological changes happening to the different mating types. For example, in *C.*
330 *deneoformans* the MATα cell responds to pheromone by forming conjugation tubes while the

331 MATa cells become enlarged (Wickes, 2002). To the best of our knowledge, these pre-
332 cellular fusion structures have been observed only in *C. deneoformans* and are defined by
333 their MAT locus (McClelland et al., 2004, Kwon-Chung et al., 2014, Fu and Heitman, 2017).
334 If this pre-cellular fusion morphology occurs in *C. neoformans*, it's possible that in the mating
335 permissive competitive scenario with the *ham1*Δa strain, the WT MATα mating partner is able
336 to produce conjugation tubes and effectively seek the MATa mutant partner. This would not
337 happen with the *ham1*Δα strain seeking the WT MATa partner, explaining the different
338 results. This also highlights the possibility that *HAM1* may have a greater effect on MATα
339 strains relative to MATa ones. This would not be a new concept. A previous study looking at
340 the global transcriptional repressor *TUP1* found mating-type specific phenotypes (Lee et al.,
341 2005). Disruption of *TUP1* led to different gene expression profiles in MATα vs MATa despite
342 having very similar cellular fusion and filamentation phenotypes (Lee et al., 2005). This
343 finding implies that even amongst lab strains there is heterogeneity with respect to
344 competitive fitness depending on the MAT locus, and that not all WT strains will behave the
345 same when in a competitive environment.

346 We wondered if *HAM1* was acting on the pheromone MAP kinase pathway, but we were
347 unable to obtain clear results from the qRT-PCR. This was not surprising given that serotype
348 A strains do not respond to mating signaling uniformly or at the same time, hence the RNA
349 samples represent a mixture of states where mating cells are a minority. Still, we saw a
350 consistent trend where *HAM1* was repressed on V8 early on, as expected if acting as a
351 negative regulator of mating. While mating is predominantly controlled by the pheromone
352 response pathway, previous studies have shown that calcineurin signaling is essential for
353 mating, haploid fruiting and spore production (Chow et al., 2017, Cruz et al., 2001). Hence,
354 we tested a potential involvement of *HAM1* in that pathway by assessing sensitivity to calcium
355 stress. We found no defects with our *ham1*Δ mutants and concluded that *HAM1* is likely not
356 involved in calcineurin signaling (Supplemental 3).

357 One of the hallmarks of mating in *C. neoformans* is the morphological transition from yeast
358 to hyphae. The hyphal form of *C. neoformans* has been shown to be unable to cause disease
359 in a mammalian host in part because it induces an immune response shift from a disease
360 permissive TH-2 to a disease protective TH-1 proinflammatory response. When examining
361 previously published RNA-seq data, we noted that *HAM1* transcripts were some of the
362 highest induced in cryptococcosis patients (Yu et al., 2021, Chen et al., 2014). This finding

363 is intriguing for two reasons. First, it lends support to the idea that to prevent a morphological
364 transition in this low nutrient environment negative regulators of mating would be highly
365 expressed. Secondly, it may indicate additional roles for *HAM1* directly related to
366 maintenance of virulence factors providing further evidence of the link between mating and
367 virulence. However, our initial survey of the key virulence mechanisms did not show any
368 obvious defects in *ham1Δ* mutants. Still, we decided to take a closer look at the capsule
369 since, as a downstream target of Pfa4, it's possible that *ham1*Δ may share defects related to
370 the cell wall or capsule as exhibited by the *pfa4*Δ mutant. Additionally, since one of the major
371 phenotypes in the *ham1Δ* relates to filamentation, we wanted to investigate if there was a
372 possible cross over between the cellular circuits governing morphology and capsule
373 production and maintenance.

374 Although capsule induction was similar, *ham1*Δ mutants exhibited a defect in capsule
375 attachment and shedding. This was similar to phenotypes exhibited by *pbx1*Δ and *pbx2*Δ
376 strains, both mutants with abnormal capsule structure (Liu et al., 2007, Kumar et al., 2014).
377 This suggested a level of involvement of *HAM1* in proper capsule formation. While defects
378 were milder than *pbx1Δ,* capsule attachment and transfer were reduced in the *ham1Δ.*
379 Capsular shedding, however, was increased in YPD, a capsule non-inducing media, and
380 trended towards higher shedding in capsule inducing medias. Capsule regulation and
381 structure during mating conditions is a topic that has received little attention. Is reasonable
382 to envision changes in capsule accompanying the morphological changes present during
383 mating. Hence, these capsule defects seen in *ham1*Δ mutants might be a consequence of
384 the abnormal mating signaling occurring in the absence of *HAM1*. Consistently, normal
385 capsule production is required for biofilm formation. Biofilm production, while not seen as a
386 virulence factor for *C. neoformans*, was likely developed as a survival tactic against
387 environmental predation (Martinez et al., 2015). The *ham1*Δα mutants have altered biofilm
388 formation, again suggesting defects in capsule attachment and altered capsule structure.
389 With all the similarities in capsule defects shared between *pbx1*Δ and *ham1*Δα, we next
390 wanted to assess the virulence capabilities of *ham1*Δ.

391 Deletion of *pbx1Δ* results in attenuated virulence in a mouse model so we expected to see a
392 similar defect in our *ham1*Δα (Liu et al., 2007). To our surprise, there were no significant
393 defects in virulence potential using the *G. mellonella* infection model relative to WT (median
394 death rate: WT, 4 days; *ham1*Δα, 5 days; and *pbx1*Δ, 6 days). Likewise, there were no

395 differences in fungal burden, even in the *pbx1*Δ-infected worms. This could be attributed to
396 the fact that they lived longer, as the burden was assessed at time of death. More detailed
397 virulence assays will be needed to confirm if there are defects in *ham1*Δ mutants affecting
398 its pathogenesis.

399 Taking all of these findings together we propose a model where *HAM1* negatively regulates
400 the mating cycle of *C. neoformans* (Fig. 10). We envision three possible locations for where
401 it could be acting: first, it could be interacting with the pheromone response pathway; second,
402 it could act directly on pheromone activated genes; and third, it could be directly involved in
403 the yeast to hyphal transition. By acting as a negative regulator of the mating cycle we believe
404 it prevents mating interactions from occurring during pathogenic conditions. This could be a
405 potential reason for why *HAM1* is so highly expressed in the CSF of cryptococcosis patients.
406 CSF is a very nutrient limited environment which may provide the right pressures for cells to
407 undergo a mating interaction, but that would be detrimental for pathogenesis.

408 By uncovering a role for *HAM1* in *C. neoformans* biology we have shown another intersection
409 point between virulence and mating. Both processes are vital to the propagation and survival
410 of the species and the presence of regulators with roles in multiple pathways reflects just
411 how important these are. Investigation of mating regulators not only improves our knowledge
412 of how the system works but also opens new avenues of investigation for therapeutic
413 interventions. Through a better understanding of fungal mating, we may be able to find more
414 intersection points between virulence and mating pathways to fully understand how these
415 two processes are connected. We hope this study serves to raise awareness about the
416 importance of mating for virulence and stirs more investigations into this phenomenon.

417 **4. Methods:**

418 **Strains and growth materials:**

419 All serotype A strains were in the KN99 background. All *ham1*Δ strains and *HAM1*-FLAG
420 tagged strain were generated using biolistic delivery (see methods below). V8 agar medium
421 was prepared using original recipe V8 juice, bacteriological grade agar and dH20. V8 medium
422 was adjusted to the appropriate pH (5 for serotype A, 7 for serotype D) using 1M hydrochloric
423 acid or sodium hydroxide tablets, respectively. 25mM $CuSO_4$ was added after autoclaving
424 before pouring plates.

425 **Fungal Genomic Manipulation:**

426 We generated all *ham1*Δ mutants using the split marker method to delete the entire *HAM1*
427 coding region. Fragments were delivered to candidate KN99α and KN99a cultures via
428 biolistic delivery (Bio-Rad PDS-1000). Deletion candidates (from at least two independent
429 transformations) were assessed using PCR as well as mating phenotype analysis to confirm
430 deletions. Two of these independent deletion mutants were tested in all mating assays. To
431 perform immunoprecipitations needed for the click chemistry analyses, a FLAG-tag strain
432 was generated using the 4x FLAG-Tag plasmid to tag the C-terminal end of Ham1. This
433 fragment with overlapping homology to the *HAM1* coding sequence was synthesized by
434 Genewiz and again delivered to candidate cells via biolistic delivery. This *HAM1*-FLAG
435 tagged strain was functional as it was indistinguishable from WT in mating and capsule
436 assays.

437 In addition to generating deletion mutants via biolistics, we also generated two independent
438 *ham1*Δa candidates via mating of KN99a with *ham1*Δα. Strains were grown in 5 mL of YPD
439 for 48 hours, spun down and washed twice in dH20, counted, and normalized to a
440 concentration of 1.5 x10^7 cells/mL. Equal cell volumes of each mating pairs were mixed and
441 incubated at RT for an hour. 100-200 uL of this mixture was spotted onto V8 mating plates
442 and incubated in the dark at RT for 7 days. Filaments from each mating interaction were
443 scraped using a sterile toothpick and resuspended in dH20. Spores were plated on YPD with
444 selection agar plates and streaked twice with selection for single colonies. Isolated single
445 colonies were tested for mating type using a mating interaction with known tester strains
446 (JEC20 and JEC21). These *ham1*Δa mutants behaved similar to the mutants generated by
447 biolistics.

448 Lastly, because we were unable to generate a complemented strain on the same loci by
449 biolistics, we also tested a commercially available *ham1*Δ deletion which we refer as C07
450 (the well number on the deletion collection plate). All 3 independent mutants showed the
451 same phenotypes.

452 **Cell preparation and protein extraction of palmitate fed cells:**

453 *HAM1*-FLAG tagged strains and KN99a strains were grown in 50 mL of YNB medium, pH
454 7.0. Once an OD of 0.5 was reached, strains were fed with 15uL of 5uM Alkynyl Palmitic Acid

455 (Click Chemistry Tools #1165) and incubated for 1hr at 30°C with shaking. Cells were
456 washed twice in cold dH_20 and flash frozen until ready for use. Cells were thawed on ice and
457 disrupted in lysis buffer (100 mM Tris-HCl pH 7.4, 0.5% Triton X-100, 150mM NaCl, 13% w/v
458 glycerol, protease inhibitor tablet, Roche) by bead beating (mini bead beater-16, Biospec
459 products #607) for 5 cycles 1 minute on 1 minute rest on ice. Cell extracts were spun down
460 at 13,000 x g for 10 minutes at 4C. Protein concentration of the supernatant was determined
461 by a detergent compatible Bradford assay (23246, ThermoFisherScientific).

462 **Immunoprecipitation and Click Chemistry:**

463 Based on the methods described in Yount et al., 2011, 1ug of protein lysates from fed and
464 unfed cell populations were incubated with 100 uL of 50% slurry of anti-FLAG M2 affinity gel
465 (A2220; Sigma-Aldrich) for 20 minutes on a nutator at 4°C. The protein-bead mixtures were
466 then loaded onto a gravity column (TALON 2 mL Disposable Gravity Column, Takara
467 #635606). Lysate was loaded into the column 5 times with gravity flow and then washed in a
468 1M NaCl buffer 3 times. Beads were then washed twice with 150mM NaCl buffer before
469 resuspended in Click Chemistry buffer according to the manufacturer's protocol (#1262, Click
470 Chemistry Tools) apart from the AFDye 680 Azide Plus reporter (Click Chemistry Tools
471 #1512) which was added at a concentration of 1.25uM. Excess reactants were removed by
472 spinning down anti-FLAG M2 affinity gel and washing twice in 1x PBS. Beads were then
473 resuspended in 1x Laemmli Buffer and heated at 70°C for 10 minutes. After SDS-PAGE the
474 10% polyacrylamide gel was destained in Click Chemistry Destain (40% methanol, 50%
475 acetic acid, 10% water) overnight and gel visualized on an Odyssey Imaging System (LI-
476 COR Biosciences).

477 **Cellular Fusion:**

478 Cellular fusion efficiency was assessed using overnight cultures grown in YPD that were
479 washed twice in dH20. Cultures were normalized to an OD of 0.5 and resuspended in dH20.
480 Each cross is comprised of cells of opposite mating type and different antibiotic resistance
481 cassettes to determine the fusion efficiency of each cross. Equal volumes of each strain are
482 mixed for their respective crosses and spotted in 50uL increments on V8 mating agar. Each
483 cross is spotted in triplicate and left to dry for 20 minutes. Once all plates were dry, they were
484 transferred to a mating chamber (DM1, Mycolabs) and left in the dark for 5 days at ambient
485 room temperature with a relative humidity of 40-50%. After incubation, each cross was

486 scraped and resuspended in 1 mL of dH20 and normalized via cell count to $1x10^7$ cells/mL.
487 For quantification, 100 uL of undiluted, or 10 and 100-fold dilutions of the $1x10^7$ cells/mL
488 suspension, was plated on both double and single antibiotic YPD resistance plates (NAT and
489 NEO). Once plates were dry, they were transferred to a 30°C room, incubated for three to
490 four days, and counted for CFUs.

491 **Hyphal staining:**

492 Single colonies from mutant crosses were scraped and resuspended in dH20. Colonies were
493 then stained with either 5 ug/mL DAPI or 100 ug/mL Calcofluor White (CFW) and incubated
494 at 30°C in the dark for 20 minutes. Cells were then washed three times in 1x PBS and
495 resuspended in 100 uL. Cells were then imaged using a 100x oil immersion objective in a
496 Zeiss Axio Observer microscope.

497 **Assessment of Bisexual Mating:**

498 Adapted from bisexual mating protocol from Sun et al., 2019. Briefly, strains were grown
499 overnight in YPD, washed twice in dH20 and normalized to an OD of 1. Cells of opposite
500 mating type for each cross were mixed in equal amounts in a separate tube and subsequently
501 spotted in 20 uL amounts onto V8 agar plates. All crosses were spotted in triplicate and left
502 to dry for 20 minutes. Once all plates were dry, they were transferred to a mating chamber
503 (DM1, Mycolabs) and left in the dark for up to 4 weeks with a relative humidity of 40-50%.

504 **Cellular Competition Assessment:**

505 Each cross consists of three strains: two of the same mating type but with opposing antibiotic
506 resistance cassettes (competitor strains), and one of the opposite mating type with no
507 antibiotic resistance (donor strain). Overnight cultures for each strain were grown in YPD until
508 log phase. Cultures were then washed twice in dH20, counted, and normalized to a
509 concentration of $1x10^5$ cells/ml. Competitor and recipient strains were mixed in equal
510 amounts for each cross. 30 uL of each cross was plated in triplicate on V8 and YPD medium
511 and left to dry for 20 minutes. Once all plates were dry, they were transferred to a mating
512 chamber and left in the dark for 10 days with a relative humidity of 40-50%. After the 10 days
513 crosses were scraped and resuspended in dH20. Crosses in YPD were diluted 100,000x and
514 crosses in V8 were diluted 10,000x. 100 uL of the respective dilutions was plated in single

515 antibiotic supplemented YPD plates (NAT or G418). Plates were incubated for 2-3 days and
516 imaged for CFUs counting using a Bio-Rad Gel Doc EZ imager.

517 **RNA isolation from bisexual mating crosses:**

518 Bisexual mating crosses are set up as previously described and allowed to incubate for 1, 3,
519 5 and 7 days. Cells are then harvested, washed once in dH20, washed with RNA stop
520 solution and flash frozen and stored at -80°C until ready for extraction. A TRIzol-extraction
521 (Life Technologies #15596-026) protocol is used followed by an RNA clean up step using the
522 ZYMO RNA Clean and Concentrator kit (cat # R1019). Up to 1ug of RNA is then converted
523 into cDNA using the NEB LunaScript® RT Supermix Kit (NEB #E3010) followed by qPCR
524 using the NEB Luna Universal qPCR Master Mix (NEB #M3003). The $\Delta\Delta_{CT}$ method was used
525 for quantification of relative transcript level normalized to YPD samples (Livak and
526 Schmidttgen 2001).

527 **Capsule induction and visualization with India Ink:**

528 Cultures were grown overnight in 5 mL of YPD medium. Cultures were spun down at 3,000
529 x g for 5 minutes and resuspended in 1 mL of PBS. After cell count, $1x10^7$ cells/ml were
530 transferred to a new microtube and pelleted. Pellet was resuspended in 1 mL of Dulbelcco's
531 Modified Eagle's Medium (DMEM) (Corning; VWR 45000-304). This suspension was diluted
532 10-fold by adding 500 uL to 4.5 mL of DMEM to a final concentration of $1x10^6$ cells/mL. 1 mL
533 aliquots of this cell suspension were added into a 24 well culture plate and incubated at 37°C
534 with 5% CO_2 for 24 hours. After 24-hour incubation, samples were transferred to microtubes
535 and spun down at 3,000 x g for 5 minutes. Samples were washed in PBS and resuspended
536 in a final volume of 50 uL. In a separate tube, 10 uL of sample were mix wth India Ink and a
537 drop of the mixed sample and India ink was pipetted onto a Polylysine-coated slide and
538 imaged on a Zeiss Axio Observer Microscope.

539 **Capsule Sonication:**

540 Capsule is induced as described above and cells were resuspended in 1 mL of 1x PBS. A
541 portion of the cells was aliquoted (unsonicated controls) and the rest were subjected to
542 sonication using a tip sonicator (Branson #SFX250) at 20% power with 0.5 pulse for 20s and
543 kept on ice. Once all strains had been sonicated, all samples were mixed with India ink as

544 described above and visualized on a Zeiss Axio Observer Microscope at 100x oil immersion
545 magnification. The capsule radius was measured using FIJI (Abramhoff et al., 2004).

546 **Capsule Transfer:**

547 Capsule transfer assays were performed as previously described (Kumar et al., 2014).
548 Capsule donor strains were grown in 5 mL of YPD liquid culture for 5 days prior to the
549 experiment. On day 4 a *cap59Δ* acceptor culture was grown overnight. Donor cultures were
550 spun down for 5 minutes at 3,000 x g and the top 1.5 mL was filtered through a 0.22μm filter
551 (Avantor #76479-024). 1 mL from this filtration step was heated at 70C to create conditioned
552 media. Acceptor cells were washed twice with 1x PBS and counted on a Bio Rad TC20
553 automatic cell counter and diluted to final concentration of $5x10^6$ cells/mL in a volume of
554 400ul. Conditioned media was added in the appropriate dilution to acceptor cells and
555 incubated for 1hr with gentle rotation. Cells were pelleted at 3000 x g for 5 minutes and
556 washed twice with 1x PBS. Resuspend cells in a volume of 100 uL and added Cy3
557 conjugated 3C2 anti GXM antibody to a final concentration of 8ug/ml. Incubated for 1 hour
558 with gentle rotation. Cells were pelleted at 3000 x g for 5 minutes and washed twice with 1x
559 PBS. Cells were resuspended in 100 uL and 100 ug/mL concentration of CFW was added
560 and incubated for 20-30 mins with gentle rotation. Cells were pelleted at 3000 x g for 5
561 minutes and washed twice with 1x PBS. Cells were resuspended in a final volume of 50 uL
562 of 1x PBS.

563 **Capsule Shedding via GXM Immunoblotting:**

564 GXM immunoblotting assays were performed as previously described (Yoneda and Doering
565 2008, Denham et al., 2018). Briefly, cells were inoculated into YPD and allowed to grow for
566 24 hours. Subsequently dilutions of 1:100 were performed and cells were inoculated into the
567 desired media of interest with the exception of DMEM where $1x10^6$ cells/mL were added to
568 5 mL of fresh DMEM. Cells were then incubated in their respective medias for 3 days at 30°C
569 with shaking at 225 rpm. DMEM cultures were incubated at 37°C with 5% CO_2 to induce
570 capsule formation and subsequent shedding. After 3 days, the cultures were quantified on a
571 cell counter (Bio-Tad TC20), and the whole culture were spun down for 5 minutes at 3000 x
572 g. The top 1.5 mL was filtered through a 0.22μm filter. 1 mL from this filtration step was
573 heated at 70°C for 10 minutes to create conditioned media. Subsequent conditioned media
574 was loaded onto a 0.6% Megabase agarose gel (BioRad #1613108) and run for 8-10 hr at

575 40V. To normalize the amount of GXM loaded onto the gel, cell counts were taken for each
576 strain in each media. The amount of GXM loaded was normalized to the lowest cell count in
577 a total volume of 100 ul. When the dye front was at the bottom of the gel, the electrophoresis
578 was stopped and the gel used to assemble the immunoblot sandwich. Using a Nylon
579 membrane, the sandwich was assembled as follows, starting from the bottom: wick, 3 pieces
580 of thick blotting paper, gel, membrane, 3 pieces of blotting paper, and paper towels (approx.
581 5 cm in height). The immunoblot sandwich was incubated with a 20x Sodium Citrate buffer
582 for 10-12 hours or until all the paper towels were saturated. The membrane was blocked for
583 48 hours in 1× TBS-5% milk and incubated for 1 h in 1×TBST-1% milk with 1 µg/mL of anti-
584 GXM monoclonal antibodies F12D2 and 1255. The membrane was rinsed three times in 1×
585 TBST and incubated for 1 h in 1× TBST-1% milk with Odyssey antibody at 1:10,000. The
586 membrane was rinsed again three times in 1× TBST and imaged on the Odyssey Imaging
587 System (LI-COR).

588 **Capsule Shedding via ELISA:**

589 GXM ELISA was done as described using a kit by IMMY-Labs (#CRY 101) (Denham et al.,
590 2018). Conditioned media from cells was obtained as described above for GXM
591 immunoblots. Conditioned media was diluted by a factor of $1x10^{-4}$ and $1x10^{-6}$ using serial
592 dilutions due to the sensitivity of the assay. Lyophilized GXM was provided by the Brown Lab
593 at the University of Utah and diluted to a concentration of 2mg/mL and working stocks were
594 generated. The highest standard used in the ELISA was 78 ng/ml.

595 **XTT Biofilm Assay:**

596 Assay was performed as previously described (Pierce et al., 2008). Strains were grown
597 overnight in YPD, cells were then counted (Bio-Rad TC20 automatic cell counter) and diluted
598 to $1x10^{7}$ cells/mL in DMEM, and 100uL of all of cell suspension was seeded into wells of a
599 microtiter plate. Plates were incubated at 37ºC + 5% CO_2 for 48 hr, washed with 1x PBS
600 using a microtiter plate washer (405LS, Agilent), and 100 µl of XTT/menadione solution
601 (Sigma) was added to each well. The plates were incubated for 3 hr and 75 µL of the
602 supernatant was removed and transferred to a new microtiter plate. Plates were read in a
603 microtiter plate reader at 490 nm.

604 **Uptake Assay:**

605 Uptake assays were performed as previously described (Santiago Tirado et al., 2015). PMA-
606 differentiated THP-1 cells were incubated with Lucifer Yellow-stained fungal cells that had
607 been opsonized with 40% Human serum collected from healthy donors (approved by the
608 Notre Dame Institutional Review Board (IRB) as a non-human subject research procedure).
609 After incubation for 1 hour at 37°C with 5% CO_2, plates were washed with 1x PBS using a
610 microplate washer (405LS, Agilent). Cells were then fixed with 4% Formaldehyde and stained
611 with DAPI (Sigma) and Cell Mask (Invitrogen). NaN_3 in PBS was added to the plates and
612 imaged on a Zeiss Axio Observer Microscope with an automatic stage. Each well was imaged
613 using a 3x3 grid set up and resulting images were analyzed using a Cell Profiler pipeline to
614 determine the Phagocytic Index (PI, # of internal cells per 100 THP-1) values.

615 **Infections with *Galleria mellonella*:**

616 *G. mellonella* third instar larvae were sorted and weighed as described (Stempinksi et al.,
617 2022). Larvae weighing 200 mg and above were used in the following infection assay.
618 Overnight cultures were grown and measured for an OD of 0.5-1. Cells were then washed
619 twice in 1x PBS and counted using a cell counter. A total inoculum of $1x10^5$ cells/larvae was
620 used in a total of 5uL. The back larval prolegs were swabbed with 70% Ethanol and 5uL of
621 culture was injected into the back right proleg using a Hamilton Syringe (Hamilton, #80300).
622 Syringes were sanitized and cleaned before and after each strain with both 70% Ethanol and
623 dH_2O. Survival was assessed daily. At time of death, infected *G. mellonella* larvae were
624 placed in 3 mL of dH_2O in a 15 mL falcon tube. Larvae were then homogenized using a tissue
625 homogenizer (VWR #10032-336) to break down tissue. Once sufficiently homogenized,
626 worm slurry was then diluted 10,000 or 20,000x times and plated on YPD plates
627 supplemented with either Nourseothricin (NAT) and Ampicillin (AMP) or Gentecin (G418) and
628 Ampicillin (AMP). Plates were left to incubate for 2-3 days and then imaged on the Biorad EZ
629 Gel Doc imager for CFU quantification.

630 **5. Acknowledgements:**

631 We would like to thank Dr. Rebecca Wingert for the use of her microscope for mating images,
632 Dr. Patricia Champion for use of her tip sonicator, Dr. Jessica Brown and Krystal Chung for
633 their gift of purified GXM, and Dr. Scott Briggs and Smriti Hoda for training on the waxworm
634 infection model. We would also like to thank the members of the Santiago-Tirado lab for their
635 help with editing and reading this manuscript. This work was supported by institutional funds

636 from the University of Notre Dame. Research in the Santiago-Tirado lab is supported by
637 grants from the NIH (R21AI171742 and R01AI177875). We declare no conflict of interest.

638 **Supplemental methods:**

639 **Murashige-Skoog and Filamentation agar Preparation:**

640 Murashige-Skoog (MS) media preparation was done as previously described (Sun et al.,
641 2019). Briefly, 1 foil packet of MS media (Sigma #M5524) was added to 1000 mL of dH_20
642 and 16g of Agar (VWR #9002-18-0) after autoclaving 1 mL of 1000x vitamin mix (Sigma
643 #M7150) was added prior to pouring. Filamentation agar preparation was done as previously
644 described (Xu et al., 2017). Briefly, YP media was generated (10 g yeast extract, 20 g
645 peptone, 20 g agar) and added to 900ul of dH_20 and autoclaved. After autoclaving 100mL of
646 a 20% Glucosamine hydroxamine was added and plates were poured. Bisexual mating
647 scenarios were generated as previously described for V8 mating.

648 **Phenotyping:**

649 Strains were grown overnight in 5mL of YPD liquid culture diluted to an OD_{600} of 0.2 and left
650 to grow for 2 doublings. Strains were washed in 1x PBS and counted using a Biorad TC20
651 automatic cell counter and diluted to final concentration of $1x10^7$ cells/ml. Cells were then
652 serially diluted by 10-fold to a final concentration of $1x10^3$ cells/ml. 5ul of culture was spotted
653 onto the following plates: YPD, YNB, YPD with 1M NaCl, 0.5 mg/mL Caffeine, 0.1-0.3%
654 SDS, 0.35-0.5M $CaCl_2$, 0.5 mg/mL Calcofluor White (CFW) Oxidative (H_2O_2) and Nitrosative
655 Stress ($NaNO_2$). Plates supplemented with stressors were incubated at 30C for 2-3 days.
656 Plates that had no stressors were incubated at 30C and 37C to assess temperature defects.
657 All plates were imaged on the BioRad EZ Gel Doc Imager.

658 **Antifungal assessment via slant plates:**

659 Methods were followed as previously described in Winski et al., 2022. Briefly, for
660 preparation of FLC gradient plates, 20 mL of RPMI-agar are dispensed with a sterile glass
661 pipet into petri dishes that are set on an angle such that the agar solution diminishes to
662 nothing at the raised edge of the plate. The plate is kept inclined until the layer solidifies, at
663 which point the plate is set on a level surface. At this point antifungals Fluconazole (FLC)
664 and Amphotericin B (AmpB) are added to the molten RPMI-agar and 20 mL of the agar

665 media with the FLC or AmpB are dispensed on top of the solidified layer. Once solidified
666 and dried, 500 cells in 5mL of the indicated strains were spotted across the plate from the
667 side with no FLC or Amp B to the side of highest FLC concentration.

668 **References:**

669

670 1. Abramoff, M.D., Magalhaes, P.J., Ram, S.J. "Image Processing with ImageJ".
671 Biophotonics International, volume 11, issue 7, pp. 36-42, 2004.
672 2. Barchiesi, F., Cogliati, M., Esposto, M. C., Spreghini, E., Schimizzi, A. M., Wickes, B. L.,
673 Scalise, G., & Viviani, M. A. (2005). Comparative analysis of pathogenicity of
674 Cryptococcus neoformans serotypes A, D and AD in murine cryptococcosis. *J Infect*,
675 *51*(1), 10-16. https://doi.org/10.1016/j.jinf.2004.07.013
676 3. Chen, Y., Toffaletti, D. L., Tenor, J. L., Litvintseva, A. P., Fang, C., Mitchell, T. G.,
677 McDonald, T. R., Nielsen, K., Boulware, D. R., Bicanic, T., & Perfect, J. R. (2014). The
678 Cryptococcus neoformans transcriptome at the site of human meningitis. *mBio*, *5*(1),
679 e01087-01013. https://doi.org/10.1128/mBio.01087-13
680 4. Chow, E. W., Clancey, S. A., Billmyre, R. B., Averette, A. F., Granek, J. A.,
681 Mieczkowski, P., Cardenas, M. E., & Heitman, J. (2017). Elucidation of the calcineurin-
682 Crz1 stress response transcriptional network in the human fungal pathogen
683 Cryptococcus neoformans. PLoS Genet, 13(4), e1006667.
684 https://doi.org/10.1371/journal.pgen.1006667
685 5. Crawford, C. J., Cordero, R. J. B., Guazzelli, L., Wear, M. P., Bowen, A., Oscarson, S.,
686 & Casadevall, A. (2020). Exploring Cryptococcus neoformans capsule structure and
687 assembly with a hydroxylamine-armed fluorescent probe. *J Biol Chem*, *295*(13), 4327-
688 4340. https://doi.org/10.1074/jbc.RA119.012251
689 6. Cruz, M. C., Fox, D. S., & Heitman, J. (2001). Calcineurin is required for hyphal
690 elongation during mating and haploid fruiting in Cryptococcus neoformans. EMBO J,
691 20(5), 1020-1032. https://doi.org/10.1093/emboj/20.5.1020
692 7. Denham, S. T., Verma, S., Reynolds, R. C., Worne, C. L., Daugherty, J. M., Lane, T. E.,
693 & Brown, J. C. S. (2018). Regulated Release of Cryptococcal Polysaccharide Drives
694 Virulence and Suppresses Immune Cell Infiltration into the Central Nervous System.
695 *Infection and Immunity*, *86*(3), 10.1128/iai.00662-00617.
696 https://doi.org/doi:10.1128/iai.00662-17
697 8. Dettmann, A., Heilig, Y., Valerius, O., Ludwig, S., & Seiler, S. (2014). Fungal
698 communication requires the MAK-2 pathway elements STE-20 and RAS-2, the NRC-1
699 adapter STE-50 and the MAP kinase scaffold HAM-5. *PLoS Genet*, *10*(11), e1004762.
700 https://doi.org/10.1371/journal.pgen.1004762
701 9. Fischer, M. S., & Glass, N. L. (2019). Communicate and Fuse: How Filamentous Fungi
702 Establish and Maintain an Interconnected Mycelial Network [Review]. *Frontiers in*
703 *Microbiology*, *10*. https://doi.org/10.3389/fmicb.2019.00619
704 10. Fisher, M. C., Gurr, S. J., Cuomo, C. A., Blehert, D. S., Jin, H., Stukenbrock, E. H.,
705 Stajich, J. E., Kahmann, R., Boone, C., Denning, D. W., Gow, N. A. R., Klein, B. S.,
706 Kronstad, J. W., Sheppard, D. C., Taylor, J. W., Wright, G. D., Heitman, J., Casadevall,
707 A., & Cowen, L. E. (2020). Threats Posed by the Fungal Kingdom to Humans, Wildlife,
708 and Agriculture. *mBio*, *11*(3). https://doi.org/10.1128/mBio.00449-20
709 11. Fu, C., & Heitman, J. (2017). PRM1 and KAR5 function in cell-cell fusion and
710 karyogamy to drive distinct bisexual and unisexual cycles in the Cryptococcus
711 pathogenic species complex. *PLoS Genet*, *13*(11), e1007113.
712 https://doi.org/10.1371/journal.pgen.1007113

713 12. Fu, C., Sun, S., Billmyre, R. B., Roach, K. C., & Heitman, J. (2015). Unisexual versus
714 bisexual mating in Cryptococcus neoformans: Consequences and biological impacts.
715 *Fungal Genet Biol*, *78*, 65-75. https://doi.org/10.1016/j.fgb.2014.08.008
716 13. Fu, C., Thielhelm, T. P., & Heitman, J. (2019). Unisexual reproduction promotes
717 competition for mating partners in the global human fungal pathogen Cryptococcus
718 deneoformans. *PLoS Genet*, *15*(9), e1008394.
719 https://doi.org/10.1371/journal.pgen.1008394
720 14. Heitman, J., Allen, B., Alspaugh, J. A., & Kwon-Chung, K. J. (1999). On the origins of
721 congenic MATalpha and MATa strains of the pathogenic yeast Cryptococcus
722 neoformans. *Fungal Genet Biol*, *28*(1), 1-5. https://doi.org/10.1006/fgbi.1999.1155
723 15. Kumar, P., Heiss, C., Santiago-Tirado, F. H., Black, I., Azadi, P., & Doering, T. L.
724 (2014). Pbx proteins in Cryptococcus neoformans cell wall remodeling and capsule
725 assembly. *Eukaryot Cell*, *13*(5), 560-571. https://doi.org/10.1128/ec.00290-13
726 16. Kwon-Chung, K. J., Fraser, J. A., Doering, T. L., Wang, Z., Janbon, G., Idnurm, A., &
727 Bahn, Y. S. (2014). Cryptococcus neoformans and Cryptococcus gattii, the etiologic
728 agents of cryptococcosis. *Cold Spring Harb Perspect Med*, *4*(7), a019760.
729 https://doi.org/10.1101/cshperspect.a019760
730 17. Lee, H., Chang, Y. C., & Kwon-Chung, K. J. (2005). TUP1 disruption reveals biological
731 differences between MATa and MATalpha strains of Cryptococcus neoformans. *Mol*
732 *Microbiol*, *55*(4), 1222-1232. https://doi.org/10.1111/j.1365-2958.2004.04458.x
733 18. Lin, X. (2009). Cryptococcus neoformans: morphogenesis, infection, and evolution.
734 *Infect Genet Evol*, *9*(4), 401-416. https://doi.org/10.1016/j.meegid.2009.01.013
735 19. Lin, X., Jackson, J. C., Feretzaki, M., Xue, C., & Heitman, J. (2010). Transcription
736 factors Mat2 and Znf2 operate cellular circuits orchestrating opposite- and same-sex
737 mating in Cryptococcus neoformans. *PLoS Genet*, *6*(5), e1000953.
738 https://doi.org/10.1371/journal.pgen.1000953
739 20. Lin, X., Nielsen, K., Patel, S., & Heitman, J. (2008). Impact of Mating Type, Serotype,
740 and Ploidy on the Virulence of *Cryptococcus neoformans*. *Infection and Immunity*, *76*(7),
741 2923-2938. https://doi.org/doi:10.1128/iai.00168-08
742 21. Liu, O. W., Kelly, M. J., Chow, E. D., & Madhani, H. D. (2007). Parallel beta-helix
743 proteins required for accurate capsule polysaccharide synthesis and virulence in the
744 yeast Cryptococcus neoformans. *Eukaryot Cell*, *6*(4), 630-640.
745 https://doi.org/10.1128/EC.00398-06
746 22. Livak KJ, Schmittgen TD. Analysis of relative gene expression data using real-time
747 quantitative PCR and the 2(-Delta Delta C(T)) Method. Methods. 2001 Dec;25(4):402-8.
748 doi: 10.1006/meth.2001.1262. PMID: 11846609.
749 23. Martinez, L. R., & Casadevall, A. (2007). Cryptococcus neoformans biofilm formation
750 depends on surface support and carbon source and reduces fungal cell susceptibility to
751 heat, cold, and UV light. *Appl Environ Microbiol*, *73*(14), 4592-4601.
752 https://doi.org/10.1128/aem.02506-06
753 24. Maziarz, E. K., & Perfect, J. R. (2016). Cryptococcosis. *Infect Dis Clin North Am*, *30*(1),
754 179-206. https://doi.org/10.1016/j.idc.2015.10.006
755 25. Min, K., Neiman, A. M., & Konopka, J. B. (2020). Fungal Pathogens: Shape-Shifting
756 Invaders. *Trends Microbiol*, *28*(11), 922-933. https://doi.org/10.1016/j.tim.2020.05.001
757 26. Nichols, C. B., Ost, K. S., Grogan, D. P., Pianalto, K., Hasan, S., & Alspaugh, J. A.
758 (2015). Impact of Protein Palmitoylation on the Virulence Potential of Cryptococcus
759 neoformans. *Eukaryot Cell*, *14*(7), 626-635. https://doi.org/10.1128/EC.00010-15

760 27. Ning, W., Jiang, P., Guo, Y., Wang, C., Tan, X., Zhang, W., Peng, D., & Xue, Y. (2020).
761 GPS-Palm: a deep learning-based graphic presentation system for the prediction of S-
762 palmitoylation sites in proteins. *Briefings in Bioinformatics*, *22*(2), 1836-1847.
763 https://doi.org/10.1093/bib/bbaa038
764 *28.* Organization, W. H. (2022). *WHO fungal priority pathogens list to guide research,*
765 *development and public health action.*
766 29. Park, S., Patterson, E. E., Cobb, J., Audhya, A., Gartenberg, M. R., & Fox, C. A. (2011).
767 Palmitoylation controls the dynamics of budding-yeast heterochromatin via the
768 telomere-binding protein Rif1. *Proceedings of the National Academy of Sciences*,
769 *108*(35), 14572-14577. https://doi.org/doi:10.1073/pnas.1105262108
770 30. Pierce, C. G., Uppuluri, P., Tristan, A. R., Wormley, F. L., Jr., Mowat, E., Ramage, G., &
771 Lopez-Ribot, J. L. (2008). A simple and reproducible 96-well plate-based method for the
772 formation of fungal biofilms and its application to antifungal susceptibility testing. *Nat*
773 *Protoc*, *3*(9), 1494-1500. https://doi.org/10.1038/nport.2008.141
774 31. Rajasingham, R., Govender, N. P., Jordan, A., Loyse, A., Shroufi, A., Denning, D. W.,
775 Meya, D. B., Chiller, T. M., & Boulware, D. R. (2022). The global burden of HIV-
776 associated cryptococcal infection in adults in 2020: a modelling analysis. *Lancet Infect*
777 *Dis*, *22*(12), 1748-1755. https://doi.org/10.1016/S1473-3099(22)00499-6
778 32. Raudaskoski, M., & Kothe, E. (2010). Basidiomycete mating type genes and pheromone
779 signaling. *Eukaryot Cell*, *9*(6), 847-859. https://doi.org/10.1128/EC.00319-09
780 33. Santiago-Tirado, F. H., Peng, T., Yang, M., Hang, H. C., & Doering, T. L. (2015). A
781 Single Protein S-acyl Transferase Acts through Diverse Substrates to Determine
782 Cryptococcal Morphology, Stress Tolerance, and Pathogenic Outcome. *PLoS Pathog*,
783 *11*(5), e1004908. https://doi.org/10.1371/journal.ppat.1004908
784 34. Severin, F. F., & Hyman, A. A. (2002). Pheromone induces programmed cell death in S.
785 cerevisiae. *Curr Biol*, *12*(7), R233-235. https://doi.org/10.1016/s0960-9822(02)00776-5
786 35. Son, Y. E., Fu, C., Jung, W. H., Oh, S. H., Kwak, J. H., Cardenas, M. E., Heitman, J., &
787 Park, H. S. (2019). Pbp1-Interacting Protein Mkt1 Regulates Virulence and Sexual
788 Reproduction in Cryptococcus neoformans. *Front Cell Infect Microbiol*, *9*, 355.
789 https://doi.org/10.3389/fcimb.2019.00355
790 36. Sun, S., Priest, S. J., & Heitman, J. (2019). Cryptococcus neoformans Mating and
791 Genetic Crosses. *Curr Protoc Microbiol*, *53*(1), e75. https://doi.org/10.1002/cpmc.75
792 37. Tamura K, Stecher G, Kumar S. MEGA11: Molecular Evolutionary Genetics Analysis
793 Version 11. Mol Biol Evol. 2021 Jun 25;38(7):3022-3027. doi:
794 10.1093/molbev/msab120. PMID: 33892491; PMCID: PMC8233496.
795 38. Viviani, M. A., Esposto, M. C., Cogliati, M., Montagna, M. T., & Wickes, B. L. (2001).
796 Isolation of a Cryptococcus neoformans serotype A MATa strain from the Italian
797 environment. *Med Mycol*, *39*(5), 383-386. https://doi.org/10.1080/mmy.39.5.383.386
798 39. Wang, L., Zhai, B., & Lin, X. (2012). The link between morphotype transition and
799 virulence in Cryptococcus neoformans. *PLoS Pathog*, *8*(6), e1002765.
800 https://doi.org/10.1371/journal.ppat.1002765
801 40. Wickes, B. L. (2002). The role of mating type and morphology in Cryptococcus
802 neoformans pathogenesis. *Int J Med Microbiol*, *292*(5-6), 313-329.
803 https://doi.org/10.1078/1438-4221-00216
804 41. Winski CJ, Qian Y, Mobashery S, Santiago-Tirado FH. An Atypical ABC Transporter Is
805 Involved in Antifungal Resistance and Host Interactions in the Pathogenic Fungus
806 Cryptococcus neoformans. mBio. 2022 Aug 30;13(4):e0153922. doi:
807 10.1128/mbio.01539-22. Epub 2022 Jun 21. PMID: 35726920; PMCID: PMC9426558.

808 42. Yoneda, A., & Doering, T. L. (2008). Regulation of Cryptococcus neoformans capsule
809 size is mediated at the polymer level. *Eukaryot Cell*, *7*(3), 546-549.
810 https://doi.org/10.1128/ec.00437-07
811 43. Xu X, Lin J, Zhao Y, Kirkman E, So YS, Bahn YS, Lin X. Glucosamine stimulates
812 pheromone-independent dimorphic transition in Cryptococcus neoformans by promoting
813 Crz1 nuclear translocation. PLoS Genet. 2017 Sep 12;13(9):e1006982. doi:
814 10.1371/journal.pgen.1006982. PMID: 28898238; PMCID: PMC5595294.
815 44. Yount JS, Zhang MM, Hang HC. Visualization and Identification of Fatty Acylated
816 Proteins Using Chemical Reporters. Curr Protoc Chem Biol. 2011 May 1;3(2):65-79.
817 doi: 10.1002/9780470559277.ch100225. PMID: 23061028; PMCID: PMC3467017.
818 45. Yu, C. H., Sephton-Clark, P., Tenor, J. L., Toffaletti, D. L., Giamberardino, C.,
819 Haverkamp, M., Cuomo, C. A., & Perfect, J. R. (2021). Gene Expression of Diverse
820 Cryptococcus Isolates during Infection of the Human Central Nervous System. *mBio*,
821 *12*(6), e0231321. https://doi.org/10.1128/mBio.02313-21
822 46. Zhai, B., Wozniak, K. L., Masso-Silva, J., Upadhyay, S., Hole, C., Rivera, A., Wormley,
823 F. L., Jr., & Lin, X. (2015). Development of protective inflammation and cell-mediated
824 immunity against Cryptococcus neoformans after exposure to hyphal mutants. *mBio*,
825 *6*(5), e01433-01415. https://doi.org/10.1128/mBio.01433-15
826 47. Zhao, Y., & Lin, X. (2021). Cryptococcus neoformans: Sex, morphogenesis, and
827 virulence. *Infect Genet Evol*, *89*, 104731. https://doi.org/10.1016/j.meegid.2021.104731
828

829 **Figures:**

A

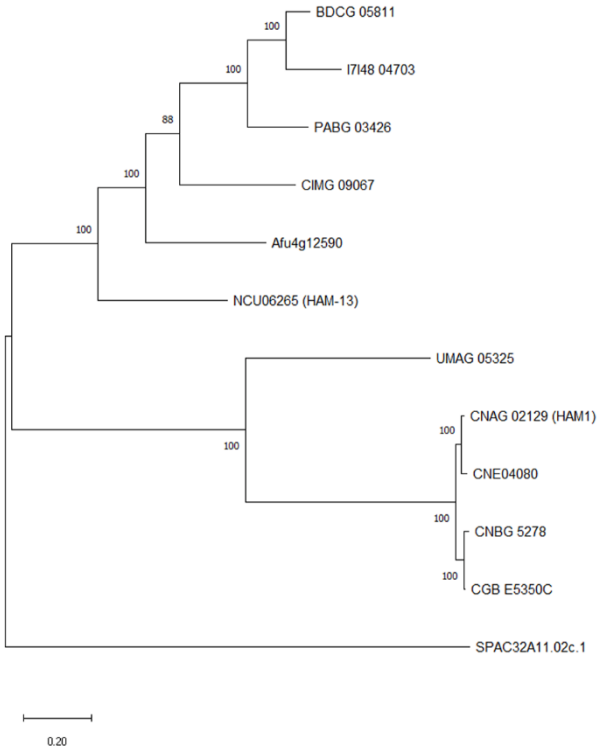

B

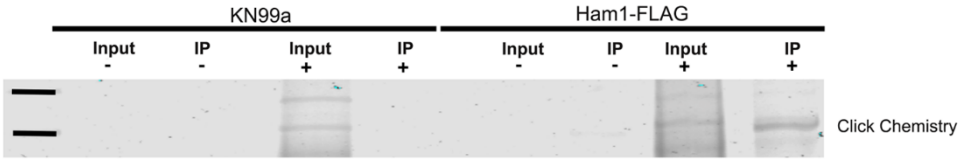

C

D

Species Name	Fungi DB Acession Number	Predicted Palmitoyation Sites	Confidence Score
Cryptococcus neoformans H99	CNAG_02129	395 559	0.878 0.775
Cryptococus deneoformans JEC21	CNE_04080	395	0.878
Cryptococcus gatti WM267	CGB_E5350C	395 559	0.878 0.775
Kwoniella bestiolae CBS 1018	I302_06570	391	0.810
Aspergillus fumigatus Af293	Afug12590	41 75	0.741 0.830
Histoplasma capsulatum G217B	I7I48_04263	400	0.809
Paracoccidioides brasiliensis Pb03	PABG_03426	400	0.894
Coccidiodies immitis RS	CIMG_09067	377	0.651
Blastomyces dermatitis ER-3	BDCG_05811	400	0.881
Ustilago maydis 521	UMAG_05325	312 410	0.837 0.819
Neurospora crassa OR74A	NCU06265	38 442	0.682 0.820

830

831 Figure 1: **Ham1 is a palmitoylated protein conserved across the fungal kingdom** A)
832 Phylogenetic tree showing conserved homologs of CNAG_02129 across common fungal
833 species. The evolutionary history of the sequences was inferred using the Maximum
834 Likelihood method with MEGAX software (Tamura et al., 2021). The tree with the highest log
835 likelihood (-10358.64) is shown. 1,000 replicate analyses (bootstraps) were run and the
836 percentage of trees in which the associated taxa clustered together is shown next to the
837 branches. B) Immunoprecipitation (IP) pull down of palmitoylated Ham1 using click
838 chemistry. Cells were either fed or not fed with an analog of palmitate then lysed and
839 underwent protein extraction. An IP was then performed on fed and unfed fractions coupled
840 with a Click chemistry experiment highlighting palmitoylated proteins. C) An accompanying
841 western blot was run on the remaining fraction not used for click chemistry. Ham1-FLAG is
842 908 aa (~100 KDa) highlighted ladder lanes are 100 and 130 KDa respectively. D) Predicted
843 palmitoylation scores of homologs found in pathogenic fungal species using GPS-Palm (Ning
844 et al., 2020) and the partially characterized homolog found in *N. crassa*. Threshold cutoff for
845 GPS palm was set to low to look at all predicted palmitoylation sites (>0.6484).
846

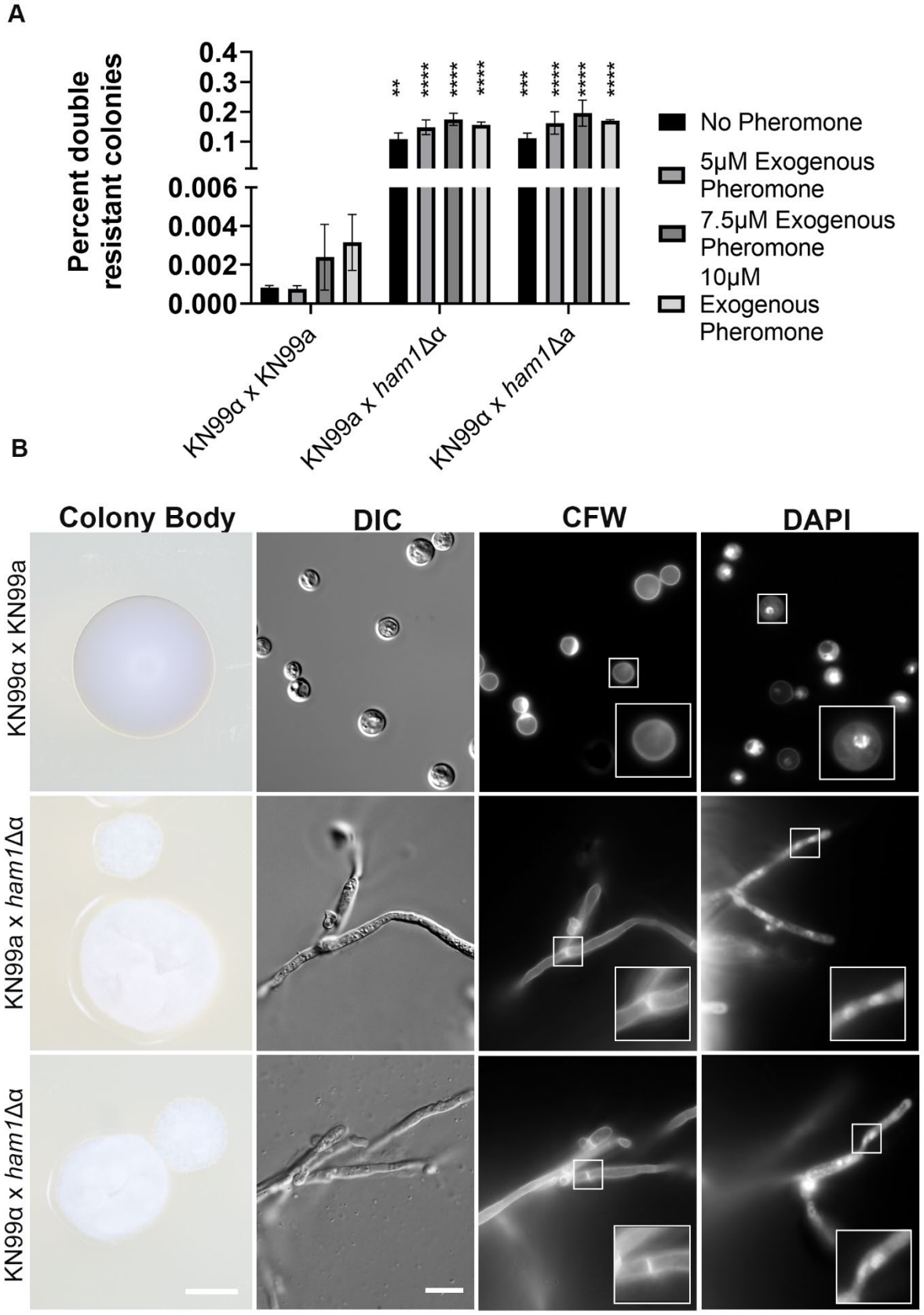
A
Percent double resistant colonies
0.4
0.3
0.2
0.1
0.006
0.004
0.002
0.000
**
****
****
****
***
****
****
****
No Pheromone
5μM Exogenous Pheromone
7.5μM Exogenous Pheromone
10μM Exogenous Pheromone
KN99α x KN99a
KN99a x ham1Δα
KN99α x ham1Δa
B
Colony Body
DIC
CFW
DAPI
KN99α x KN99a
KN99a x ham1Δα
KN99α x ham1Δα

850 Figure 2: ***ham1*Δ mutants have higher cellular fusion efficiency and exhibit dry colony**
851 **morphology** A) Percent of double antibiotic progeny resulting from bisexual crosses. 2-way
852 ANOVA with a Dunnet's multiple comparison test of WT fusion to *ham1*Δα and *ham1*Δa in
853 no pheromone and exogenous pheromone conditions ** p= 0.0012, *** p= 0.0009, ****
854 p<0.0001 n=3 biological replicates for all crosses and all conditions. B) Representative
855 images of colony body of all crosses at 2x magnification and 100x magnification of progeny
856 staining with Calcofluor white (CFW) to highlight septal divisions of hyphal form in mutant
857 crosses DAPI to show binuclear distribution in mutant crosses. Scale bars represent 50 and
858 10 microns, respectively.
859

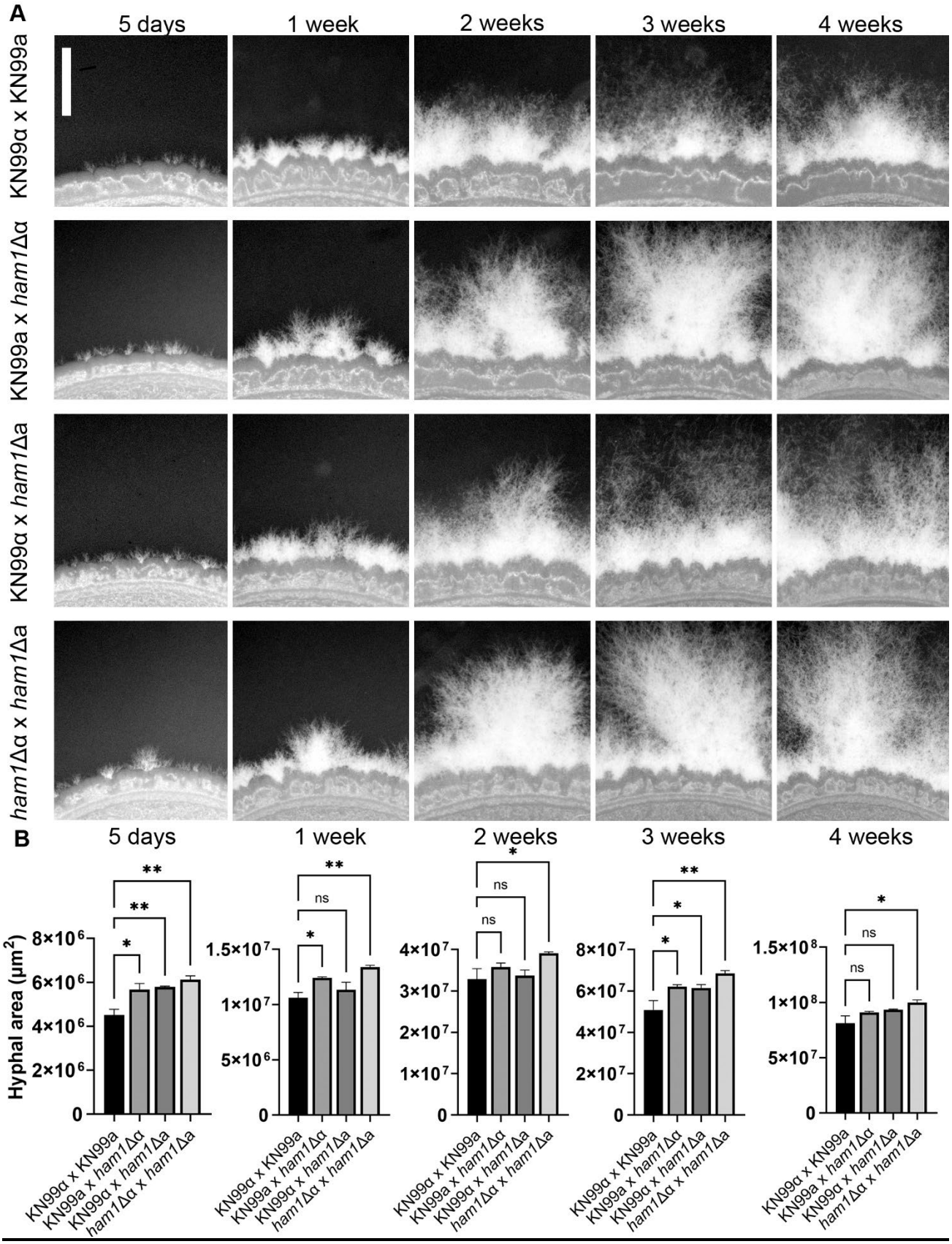
A
5 days
1 week
2 weeks
3 weeks
4 weeks
KN99α x KN99a
KN99a x ham1Δα
KN99α x ham1Δa
ham1Δα x ham1Δa
B
Hyphal area (μm²)
8×10⁶
6×10⁶
4×10⁶
2×10⁶
0
1.5×10⁷
1×10⁷
5×10⁶
4×10⁷
3×10⁷
2×10⁷
1×10⁷
8×10⁷
6×10⁷
4×10⁷
2×10⁷
1.5×10⁸
1×10⁸
5×10⁷
ns
*
**
KN99α x KN99a
KN99a x ham1Δα
KN99α x ham1Δa
ham1Δα x ham1Δa

863 Figure 3**: *ham1*Δ unilateral and bilateral crosses exhibit increased hyphal production**
864 **on V8 mating medium.** A) Representative images of WT and mutant crosses on V8 mating
865 media. All images taken at 0.63x magnification scale bar represents 1 mm. B) Quantification
866 of hyphal area for all crosses at all time points. 1-Way ANOVA with a Dunnet's multiple
867 comparison test of WT hyphal area compared to all mutant crosses * p=0.0366, ** p=0.0033.
868 n=3 biological replicates for all timepoints of hyphal area.
869

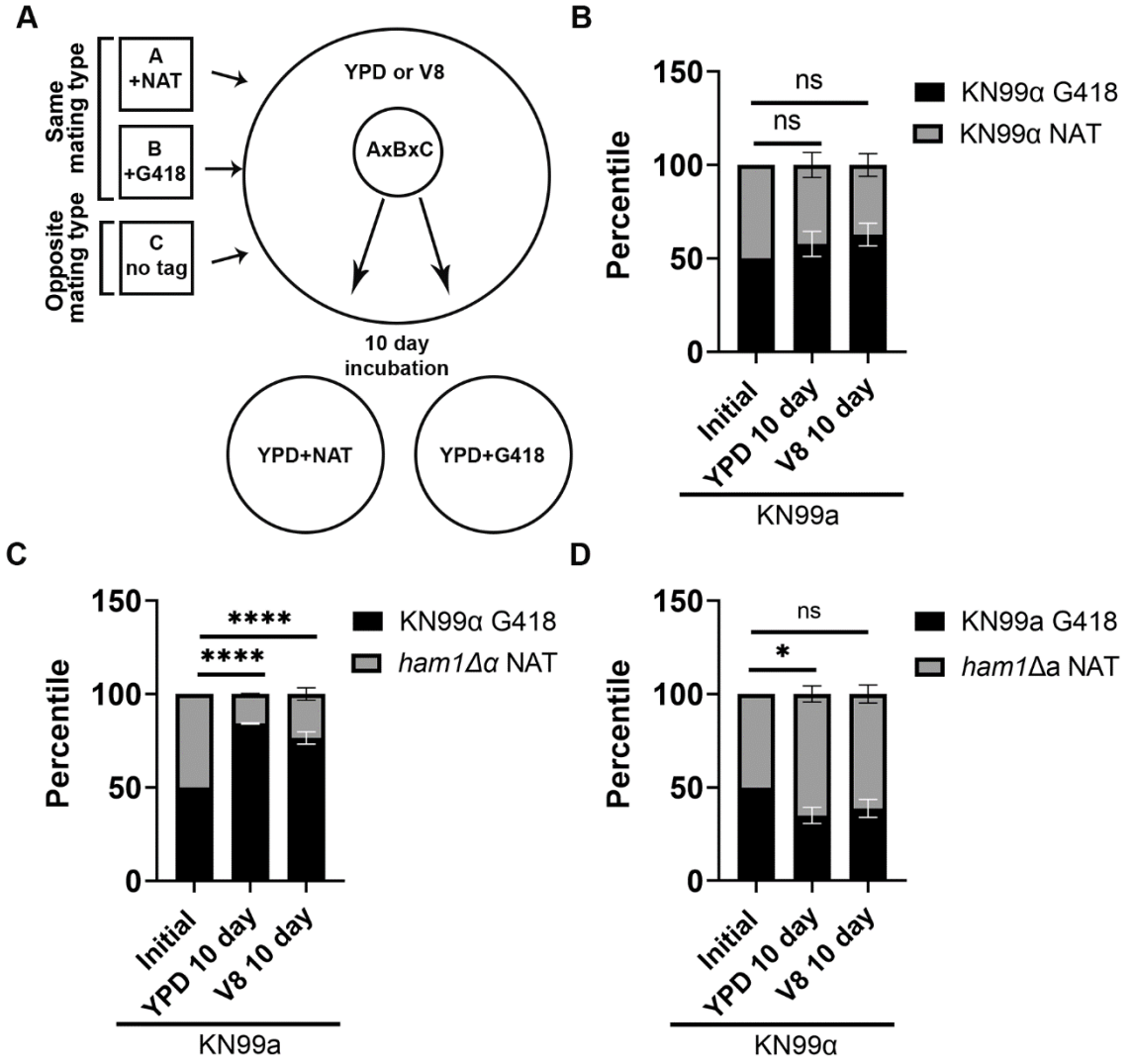

Figure 4: ***ham1*Δα has a reduced competitive fitness when compared to WT.** A) schematic of how cellular competition assay was performed. B) WT competitive fitness presented as a percentage for each cross in either YPD or V8 medium. 1-Way ANOVA with a Dunnet's multiple comparison test of KN99α NAT initial with YPD and V8 10-day percentages. C) *ham1*Δα competitive fitness presented as a percentage for each cross in either YPD or V8 medium. 1-Way ANOVA with a Dunnet's multiple comparison test of *ham1*Δα NAT initial with YPD and V8 10-day percentages **** $p<0.0001$. D) *ham1*Δa competitive fitness presented as a percentage for each cross in either YPD or V8 medium. 1-Way ANOVA with a Dunnet's multiple comparison test of *ham1*Δa NAT initial with YPD and V8 10-day percentages * $p=0.0238$. n=4 biological replicates for all competition assays.

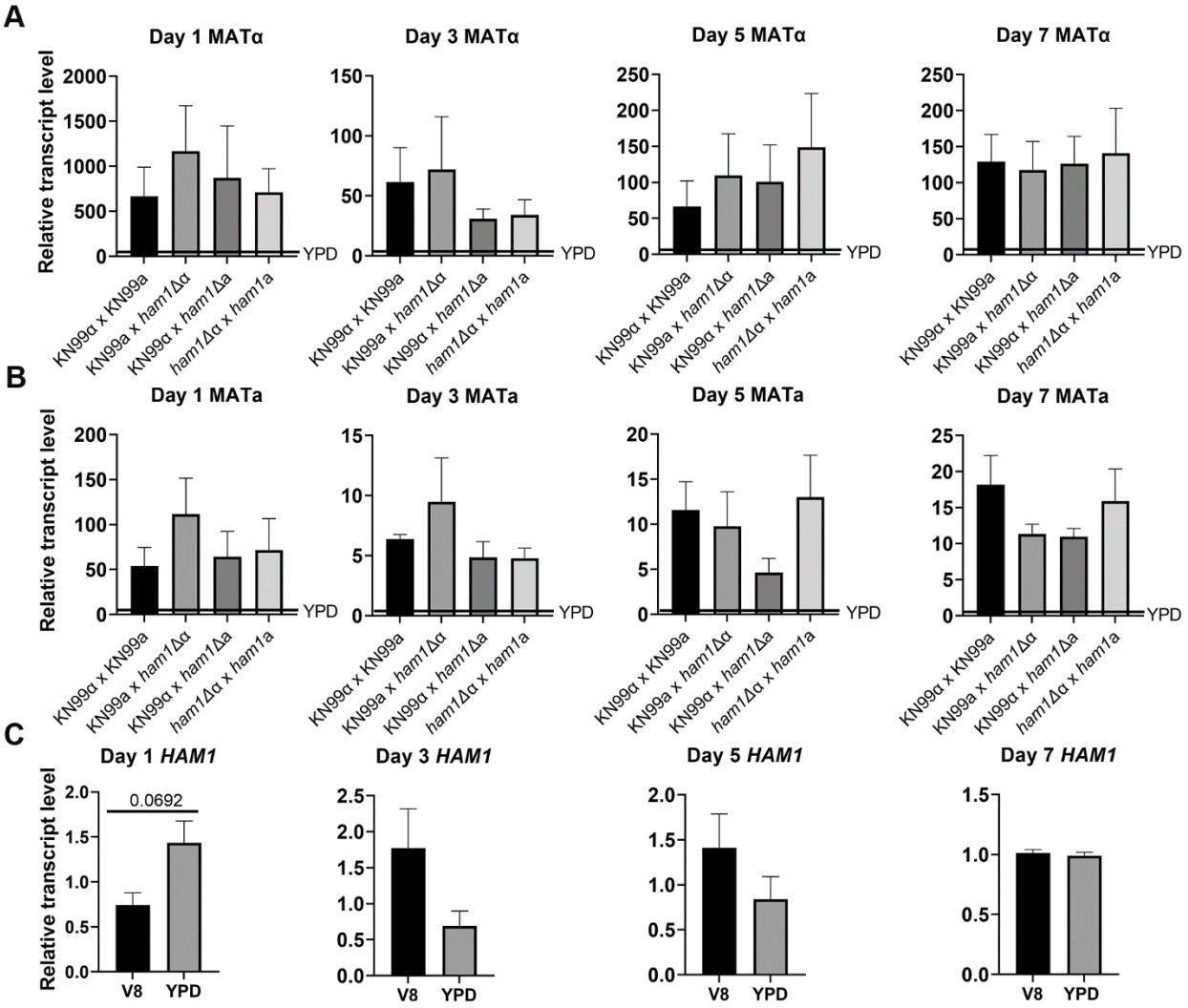

Figure 5: ***ham1*Δ exhibits similar expression of pheromone genes in mating inducing conditions over time**. A) Relative transcriptional analysis of MATα (V8 media) conditions relative to non-mating conditions (YPD media) after incubation for 1, 3, 5, and 7 days on respective medias. B) Relative transcriptional analysis of MATa in mating (V8 media) conditions relative to non-mating conditions (YPD media) after incubation for 1,3,5 and 7 days on respective medias. C) Quantification of transcript level of *HAM1* in mating and non-mating conditions after incubation for 1, 3, 5 and 7 days on respective medias. There is no significant difference between wildtype and mutant expression levels unless otherwise indicated. n=3 biological replicates for all timepoints and conditions.

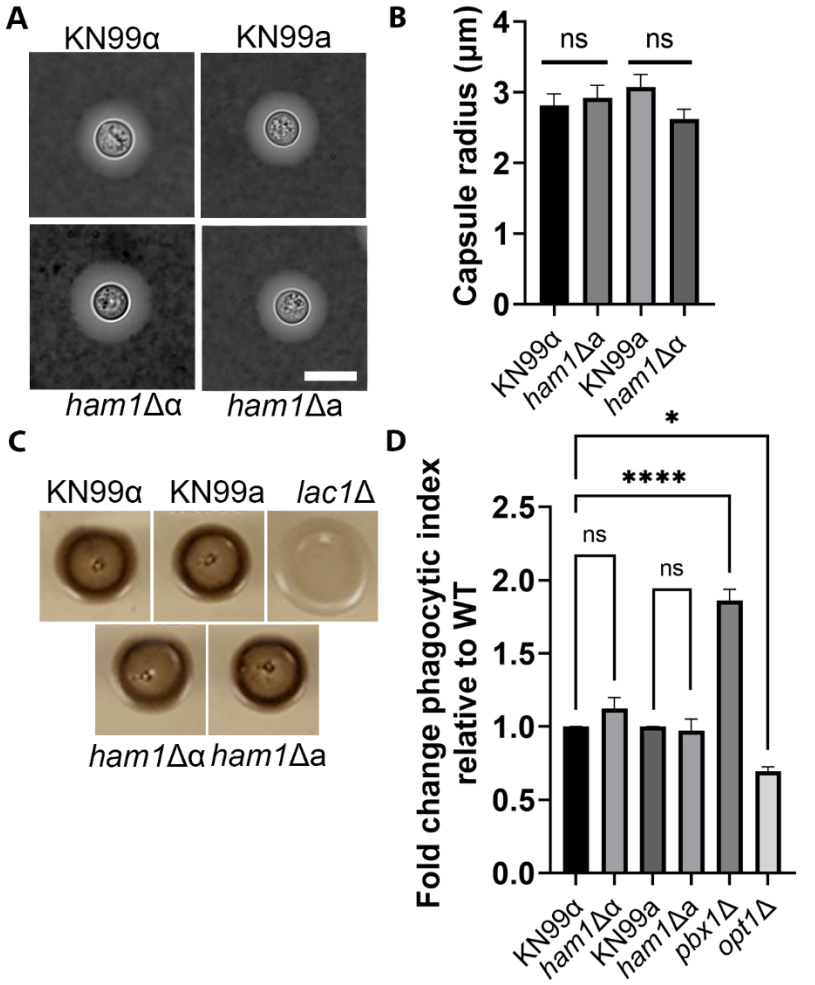

Figure 6: ***ham1*Δ shows no defects in major virulence mechanisms** A) Representative images of induced capsule stained with India Ink. Scale bar represents 10um. B) Measurement of capsule radius after induction, n=25 cells for all strains. C) Melanin induced on caffeic acid plates *lac1*Δ is a melanin mutant and serves as a negative control. D) Measurement of uptake by THP-1 phagocytic cells as a function of the number of engulfed fungi divided by the number of THP-1 cells normalized to the WT condition, *pbx1*Δ is a known mutant with a higher uptake index and *opt1*Δ is a known low uptake index. A 1-Way ANOVA test was run on all strains with the MATα background, this includes our positive (*pbx1*Δ) and negative (*opt1*Δ) controls using a Dunnet's multiple comparison test to KN99α; * p=0.0256, **** p<0.0001. A Student's t-test using a Gaussian distribution was used to compare phagocytic indices of KN99a and *ham1*Δa as they are both the MATa background.

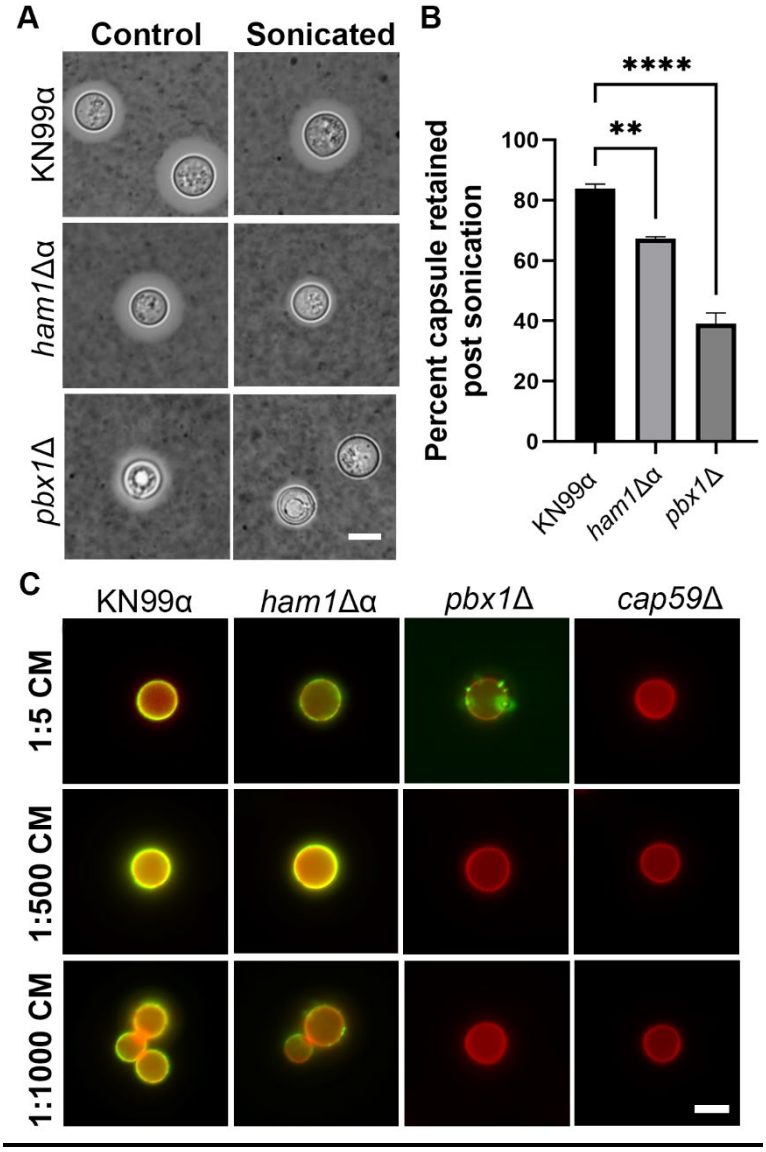

Figure 7: ***ham1*Δα exhibits defects in capsule attachment and transfer.** A) Representative images of wildtype, *ham1*Δα and *pbx1*Δ capsules stained in India Ink before and after sonication. Scale bar represents 5um. B) Quantification of the percentage of capsule retained post sonication. 1-Way ANOVA with a Dunnet's multiple comparison test to WT ** p=0.0041, **** p<0.0001 n=20 cells for all strains. C) Representative images of capsule transfer capsule visualized by conjugated 3C2 antibody with Alexa488 fluorescent probe and cell wall stained with Calcaflour white (CFW) scale bar is 10um.

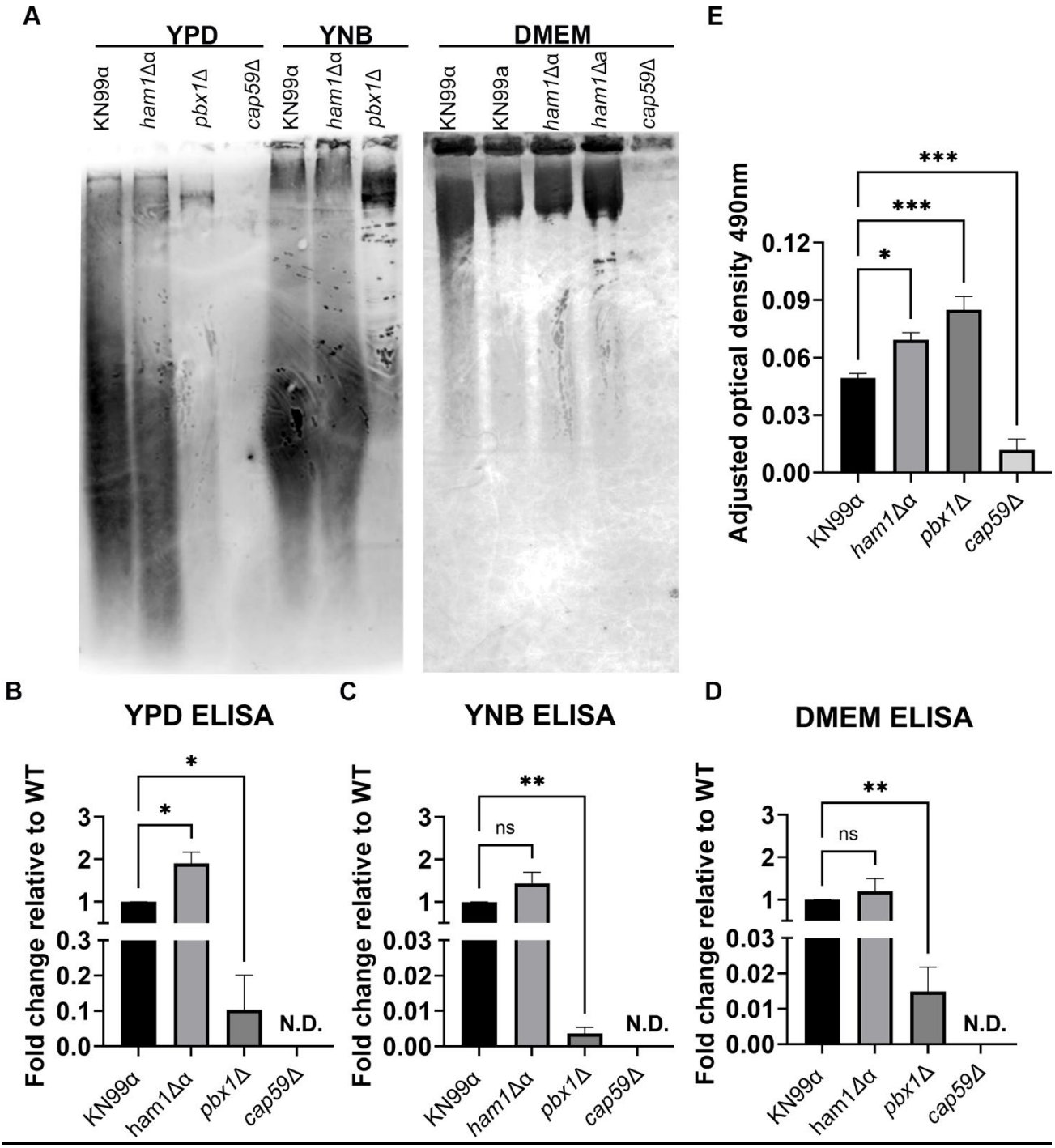
A
YPD
YNB
DMEM
KN99α
ham1Δα
pbx1Δ
cap59Δ
KN99α
ham1Δα
pbx1Δ
KN99α
KN99a
ham1Δα
ham1Δa
cap59Δ
E
Adjusted optical density 490nm
0.12
0.09
0.06
0.03
0.00
***
***
*
KN99α
ham1Δα
pbx1Δ
cap59Δ
B
YPD ELISA
Fold change relative to WT
3
2
1
0.3
0.2
0.1
0.0
*
*
N.D.
KN99α
ham1Δα
pbx1Δ
cap59Δ
C
YNB ELISA
Fold change relative to WT
3
2
1
0.03
0.02
0.01
0.00
**
ns
N.D.
KN99α
ham1Δα
pbx1Δ
cap59Δ
D
DMEM ELISA
Fold change relative to WT
3
2
1
0.03
0.02
0.01
0.00
**
ns
N.D.
KN99α
ham1Δα
pbx1Δ
cap59Δ

919
920

921 Figure 8: ***ham1*Δα exhibits increased exopolysaccharide shedding and biofilm**
922 **production** A) Representative GXM immunoblot of exopolysaccharide shedding in capsule
923 non inducing medias YPD and YNB. B) Representative GXM immunoblot of
924 exopolysaccharide shedding in capsule inducing media DMEM. C) Quantification of shed
925 exopolysaccharide in YPD via Sandwich ELISA as fold change relative to WT. A 1-Way
926 ANOVA with a Dunnet's multiple comparison test of WT to *ham1*Δ and *pbx1*Δ. * p=0.0133,
927 0.01339 respectively. D) Quantification of shed exopolysaccharide in YPD via Sandwich
928 ELISA as fold change relative to wildtype. A 1-Way ANOVA with a Dunnet's multiple
929 comparison test of WT to *ham1*Δ and *pbx1*Δ. ** p=0.0064. E) Quantification of shed
930 exopolysaccharide in DMEM via Sandwich ELISA as fold change relative to wildtype. A One-
931 Way ANOVA with a Fisher's LSD test was run on all samples ** p=0.0069. n=3 biological
932 replicates for all ELISAs.
933

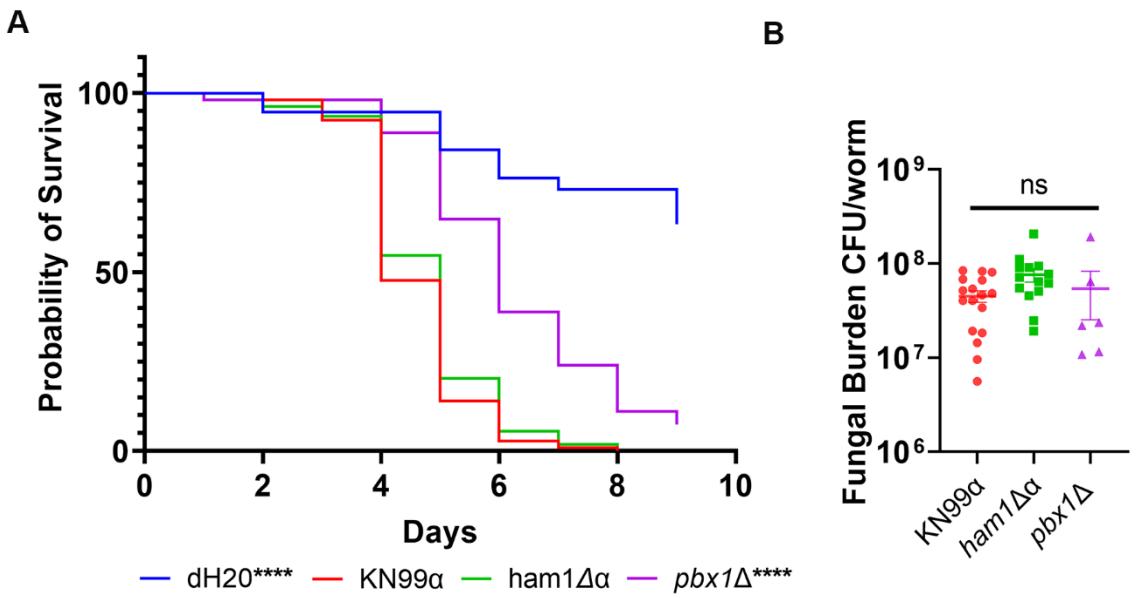

934
935
936 Figure 9**: *ham1*Δα is as virulent as WT in *G. mellonella* infections.** A) Kaplan-Meier
937 survival curve of KN99α n=107, *ham1*Δα n=108, *pbx1*Δ n=54, and dH_2O. One-Way ANOVA
938 with a Dunnet's multiple comparison test ****p<0.0001 B) Fungal burden assessment of
939 infected worms a 1-Way ANOVA was run with a Dunnet's multiple comparisons test of
940 mutants to WT was run. (KN99α n=17, *ham1*Δα n=15, *pbx1*Δ n=6)
941

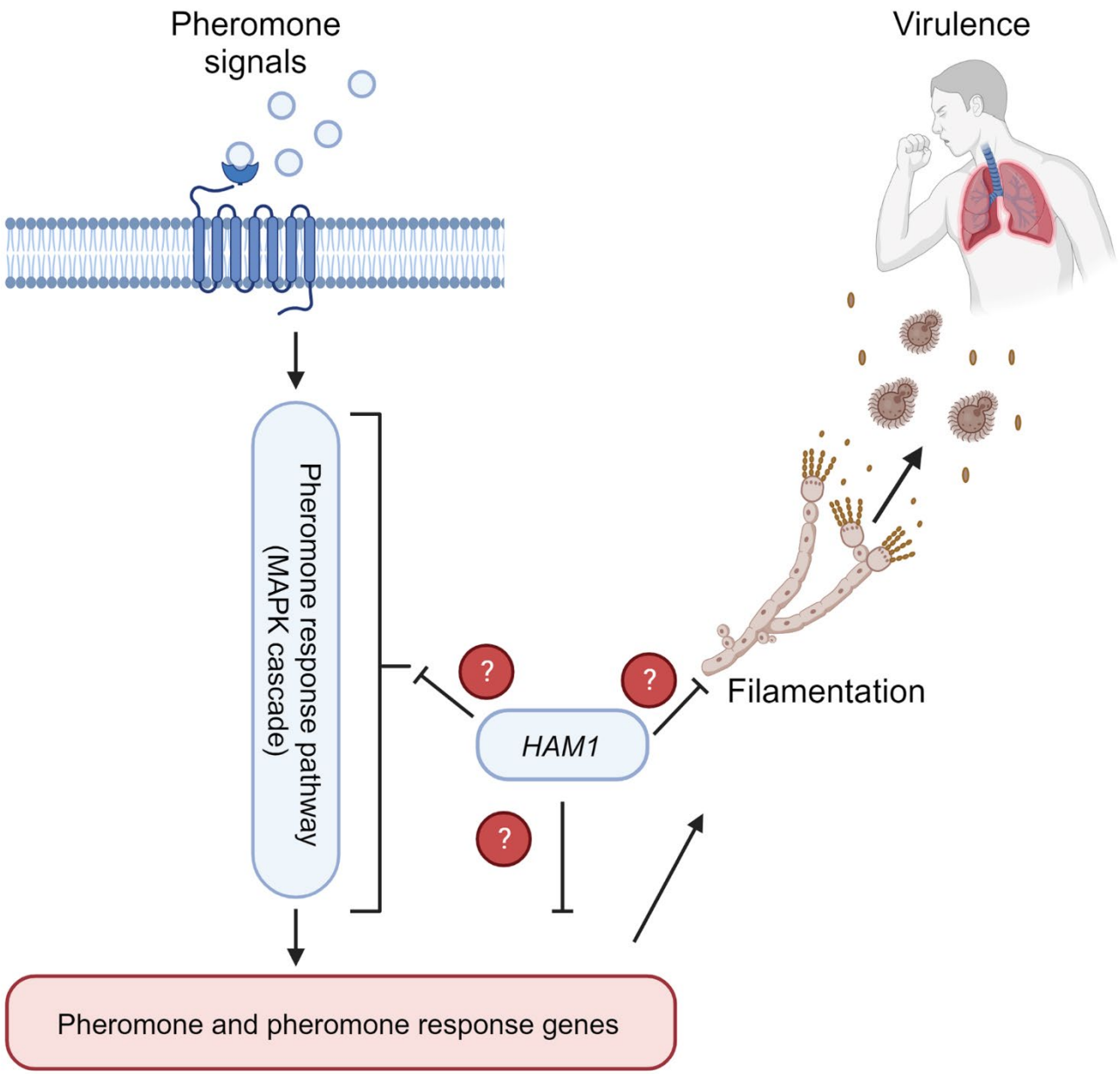

Figure 10: **Proposed model of *HAM1* involvement in *C. neoformans* biology.** Based on this study we believe that *HAM1* acts as a negative regulator in the mating cycle of *C. neoformans*. It may be acting on the pheromone response pathway, on the pheromone and pheromone response genes directly, or somehow inhibiting hyphal formation directly. During pathogenic conditions, we believe that *HAM1* is highly expressed to prevent mating from occurring due to the low nutrient environment of a mammalian host. This figure was created with BioRender.com.

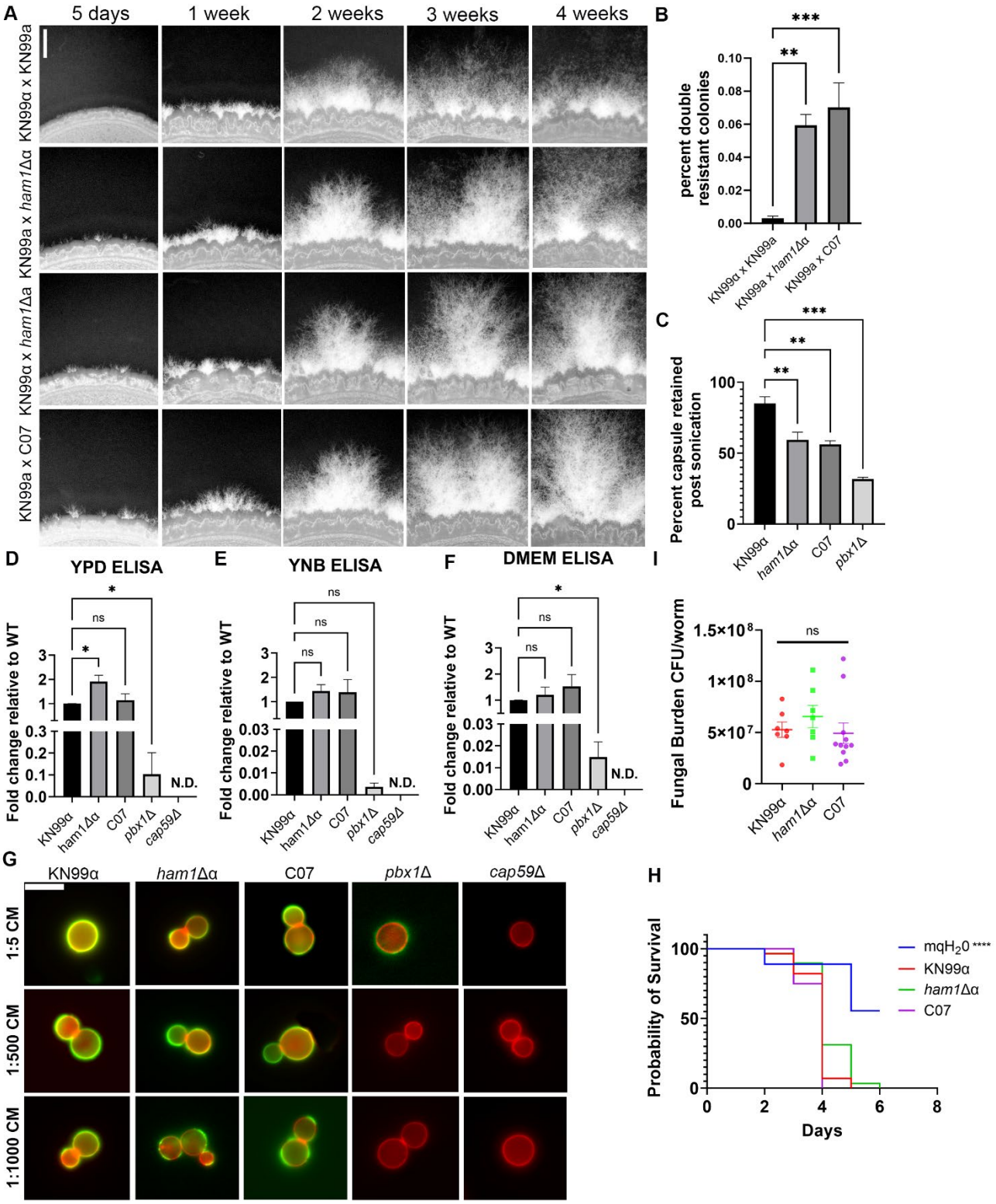
A
5 days
1 week
2 weeks
3 weeks
4 weeks
KN99α x KN99a
KN99a x ham1Δα
KN99α x ham1Δa
KN99a x C07
B
percent double resistant colonies
KN99α x KN99a
KN99a x ham1Δα
KN99a x C07
C
Percent capsule retained post sonication
KN99α
ham1Δα
C07
pbx1Δ
D
YPD ELISA
E
YNB ELISA
F
DMEM ELISA
Fold change relative to WT
N.D.
cap59Δ
I
Fungal Burden CFU/worm
ns
G
1:5 CM
1:500 CM
1:1000 CM
H
Probability of Survival
Days
mqH2O ****

954 Supplemental 1: **C07 behaves similarly to *ham1*Δ mutants in key mating and virulence**
955 **assays.** The most recent addition to the *C. neoformans* deletion collection contained a
956 deletion mutant of *HAM1* which was well number C07 (https://www.fgsc.net/). We used the
957 C07 mutant in a variety of assays where we saw phenotypes present in our *ham1*Δ mutants
958 to provide external validation of the phenotypes we were seeing. A) C07 produces hyphae
959 at a similar speed and robustness to our *ham1*Δ mutants. B) C07 produces similar amounts
960 of double resistant progeny to our *ham1*Δ mutants. A one-way ANOVA was run using multiple
961 comparisons to the WT cross. ** p=0.0014, ***p=0.0003. n=3 biological replicates for all
962 conditions C) C07 has similar defects in capsule attachment to *ham1*Δ mutants post
963 sonication. A one-way ANOVA was run using a Dunnett's multiple comparison test of all
964 mutant crosses to the WT cross ** p=0.0062 (*ham1*Δα) **, p=0.0040 (C07), ***p=0.0004. n=
965 20 cells for all conditions D) C07 trends towards shedding more capsule in non-capsule
966 inducing media YPD. A one-way ANOVA was run with a Dunnett's multiple comparisons of
967 mutants to WT *p=0.0254. E) C07 trends towards shedding more capsule in non-capsule
968 inducing media YNB. A one-way ANOVA was run with Dunnett's multiple comparisons test
969 of mutants to WT. F) C07 trends towards shedding more capsule in capsule inducing media
970 DMEM. A one-way ANOVA with a Fisher's LSD test was run on all samples * p=0.0321. n=3
971 biological replicates for all ELISAs G) C07 fails to fully transfer capsule at high dilutions
972 greater than 1:750. Representative images of capsule transfer capsule visualized by
973 conjugated 3C2 antibody with Alexa488 fluorescent probe and cell wall stained with
974 calcofluor white (CFW) scale bar is 10um. H) C07 shows no difference in survival compared
975 to WT. Kaplan-Meier survival curve of mq$H_2$0=10 KN99α n=30, *ham1*Δα n=30 and C07 n=30
976 A one-way ANOVA with a Dunnet's multiple comparison test of all conditions to WT. No
977 differences were seen in the mutants but the mq$H_2$0 survived significantly longer
978 ****p<0.0001. I) C07 shows no difference in fungal burden. KN99α n=7, *ham1*Δα n=7, C07
979 n=11. A one-way ANOVA with a Dunnet's multiple comparison test of all conditions to WT
980 was run and showed no significant difference between mutants and WT.
981

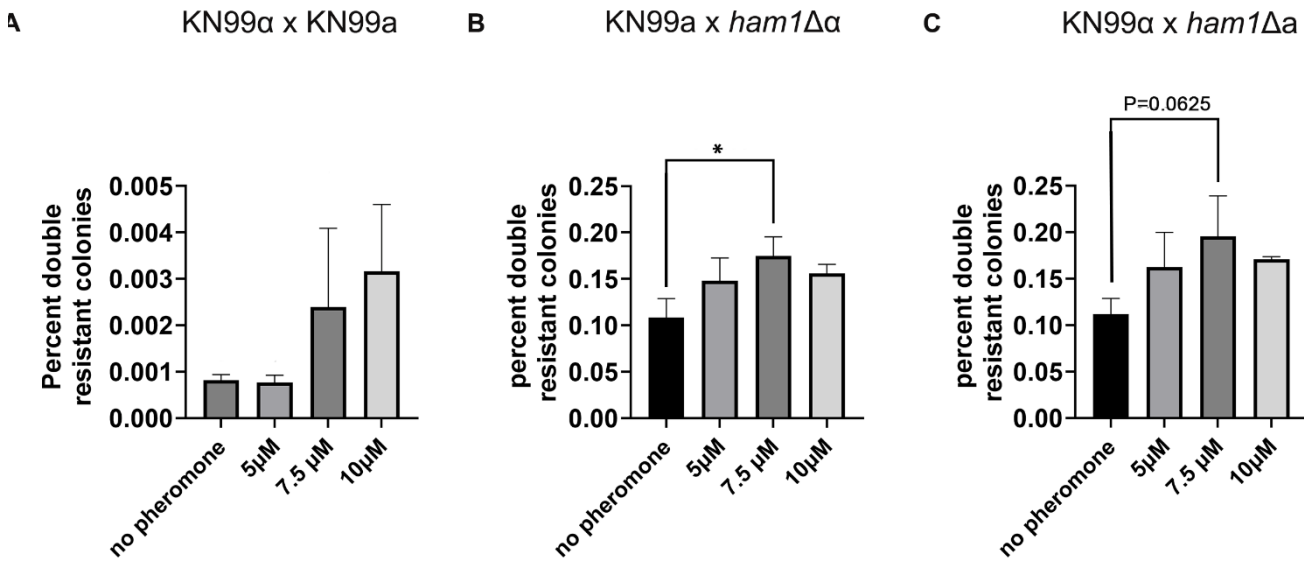

982
983 Supplemental Figure 2: **Cellular fusion comparisons with or without exogenous**
984 **pheromone addition.** A) WT cell fusion without and with 5μM, 7.5μM, and 10μM exogenous
985 pheromone. A one-way ANOVA with an LSD Fisher's test was run on all conditions, none
986 were statistically significant. B) *ham1*Δα cell fusion without and with 5μM, 7.5μM, and 10μM
987 exogenous pheromone. A one-way ANOVA with an LSD Fisher's test was run on all
988 conditions. *, P = 0.0263. C) *ham1*Δa cell fusion without and with 5μM, 7.5μM, and 10μM
989 exogenous pheromone. A one-way ANOVA with an LSD Fisher's test was run on all
990 conditions, none were statistically significant but the 7.55μM condition was approaching
991 significance, hence P value is shown. n= 3 biological replicates per condition for all cell fusion
992 assays.
993

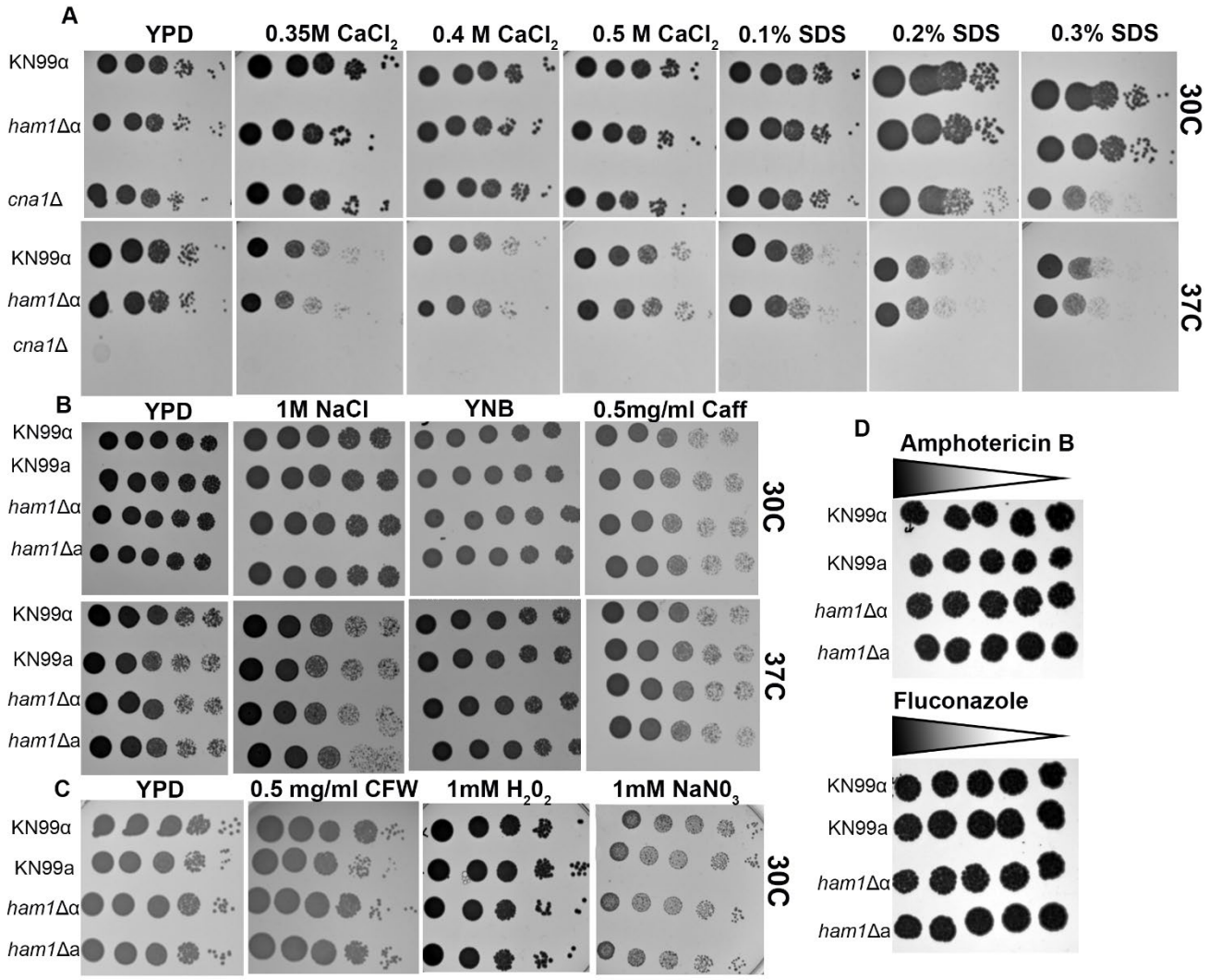

Supplemental 3: ***ham1*Δ shows no sensitivities to various cell wall and membrane stressors as well as antifungal treatments.** To rule out any issues with calcineurin signaling, cell membrane, or cell wall, we tested various conditions in YPD solid agar medium. A) Growth of indicated strains in the presence of calcium ($CaCl_2$) and sodium dodecyl sulfate (SDS) at 30°C or 37°C. B) Growth of indicated strains under thermal stress (YPD at 30 and 37C), osmotic stress (NaCl), nutrient stress (YNB), and cell wall stress signaling (Caffeine). C) Growth of indicated strains under cell wall stress (calcofluor white, CFW), oxidative stress (H_20_2) and oxidative stress ($NaNO_3$). D) Growth of indicated strains in the presence of common antifungals (Amphotericin B and Fluconazole).

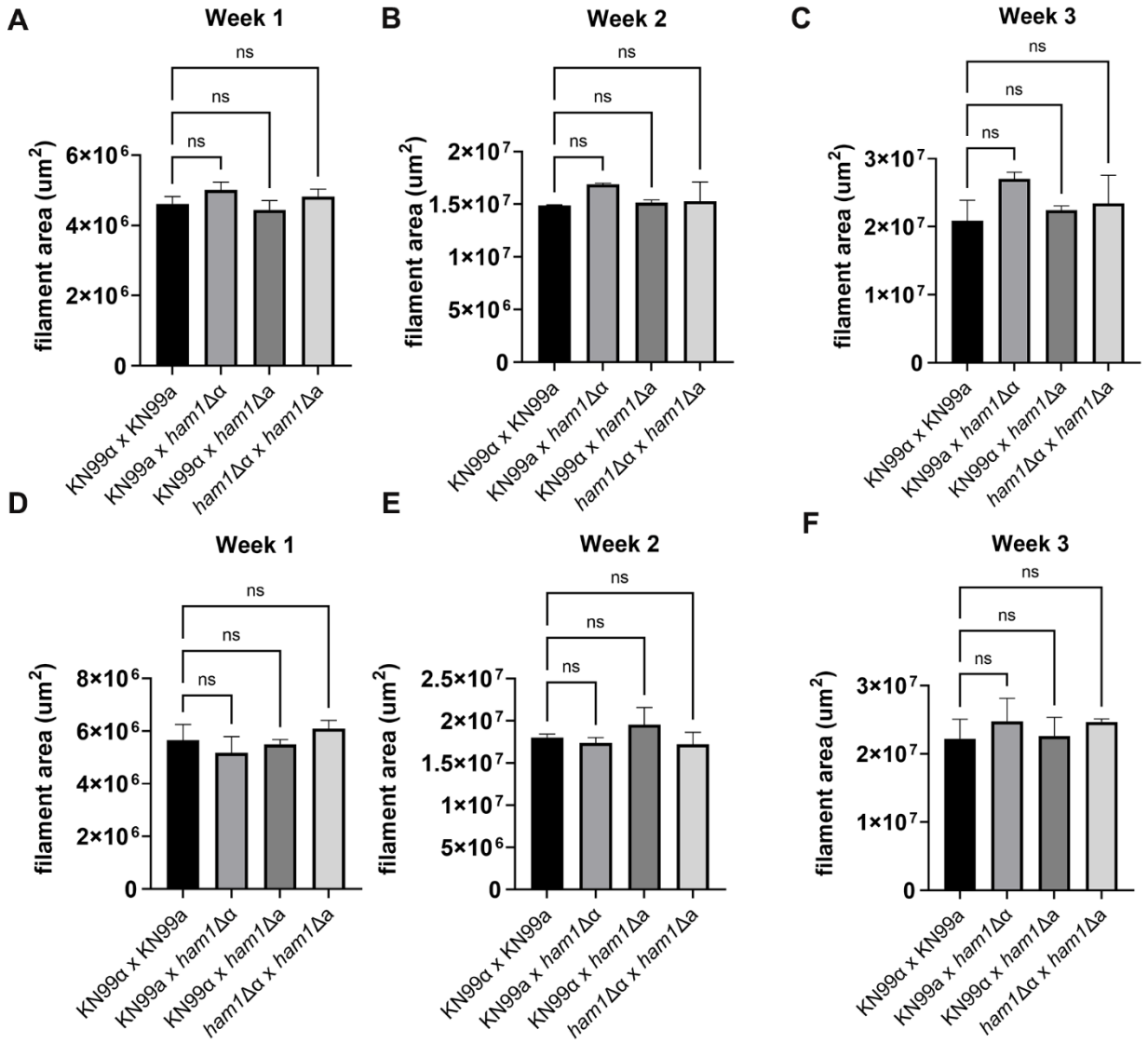

Supplemental 4: ***ham1*Δ shows no significant differences in filament area in other mating specific medias.** A-C) Filament area of WT and mutant crosses in Murashige-Skoog media. One-way ANOVA with a Dunnet's multiple comparison test of mutants to WT. D-F) Filament area of WT and mutant crosses in Filamentation Agar media. One-way ANOVA with a Dunnet's multiple comparison test of mutants to WT. No significant differences were observed.